AD-A140 695 COMPUTER SIMULATION FOR THE TRANSIENT DYNAMIC RESPONSE OF LOCKING MATERIALS(U) GEORGIA INST OF TECH ATLANTA S HANAGUD NOV 82 GIT-E-16-638 AMMRC-TR-82-60 1/1

UNCLASSIFIED DAAG46-79-C-0014 F/G 12/1 NL

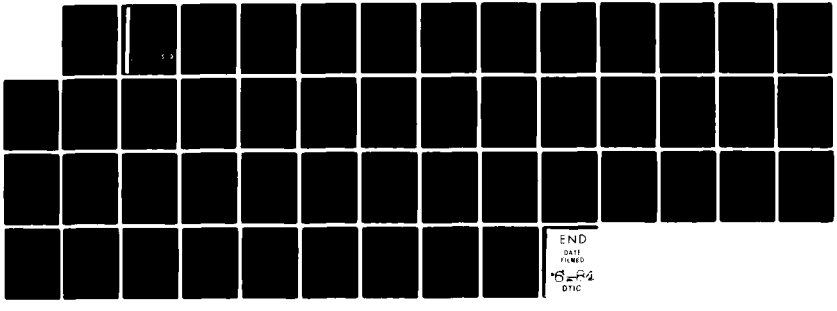

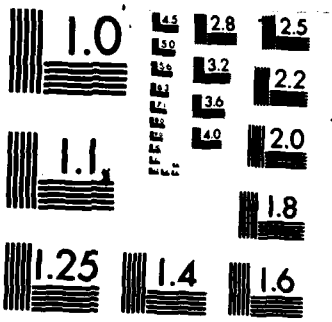

12

AD

AD-A140 695

AMMRC TR 82-60

COMPUTER SIMULATION FOR THE TRANSIENT DYNAMIC RESPONSE OF LOCKING MATERIALS

November 1982

S. HANAGUD
Georgia Institute of Technology
School of Aerospace Engineering
Atlanta, Georgia 30332

FINAL REPORT

Contract Number DAAG46-79-C-0014

Prepared for

ARMY MATERIALS AND MECHANICS RESEARCH CENTER
Watertown, Massachusetts 02172

UNCLASSIFIED

SECURITY CLASSIFICATION OF THIS PAGE (When Data Entered)

REPORT DOCUMENTATION PAGE		READ INSTRUCTIONS BEFORE COMPLETING FORM
1. REPORT NUMBER AMMRC TR 82-60	2. GOVT ACCESSION NO. AD-A120695	3. RECIPIENT'S CATALOG NUMBER
4. TITLE (and Subtitle) COMPUTER SIMULATION FOR THE TRANSIENT DYNAMIC RESPONSE OF LOCKING MATERIALS		5. TYPE OF REPORT & PERIOD COVERED Final Report - Feb 79 to Aug 81
		6. PERFORMING ORG. REPORT NUMBER E-16-638
7. AUTHOR(s) S. Hanagud		8. CONTRACT OR GRANT NUMBER(s) DAAG46-79-C-0014
9. PERFORMING ORGANIZATION NAME AND ADDRESS Georgia Institute of Technology School of Aerospace Engineering Atlanta, Georgia 30332		10. PROGRAM ELEMENT, PROJECT, TASK AREA & WORK UNIT NUMBERS D/A Project: 1L161102AH42 AMCMS Code: 611102.H420011
11. CONTROLLING OFFICE NAME AND ADDRESS Army Materials and Mechanics Research Center ATTN: DRXMR-K Watertown, Massachusetts 02172		12. REPORT DATE November 1982
		13. NUMBER OF PAGES
14. MONITORING AGENCY NAME & ADDRESS(if different from Controlling Office)		15. SECURITY CLASS. (of this report) Unclassified
		15a. DECLASSIFICATION/DOWNGRADING SCHEDULE

16. DISTRIBUTION STATEMENT (of this Report)

Approved for public release; distribution unlimited.

17. DISTRIBUTION STATEMENT (of the abstract entered in Block 20, if different from Report)

18. SUPPLEMENTARY NOTES

19. KEY WORDS (Continue on reverse side if necessary and identify by block number)

Wave propagation
Finite difference theory
Numerical analysis
Dynamic response

20. ABSTRACT (Continue on reverse side if necessary and identify by block number)

(SEE REVERSE SIDE)

DD FORM 1 JAN 73 1473 EDITION OF 1 NOV 65 IS OBSOLETE

UNCLASSIFIED

SECURITY CLASSIFICATION OF THIS PAGE (When Data Entered)

Block No. 20

ABSTRACT

The concept of a locking material and the potential effectiveness of the locking material for possible use as a countermeasure to specified mine blasts have been investigated in this report. The effectiveness of the countermeasure has been demonstrated by the use of analytical methods and second order accurate computer codes. Computer codes have been developed to investigate and evaluate such a design that uses the countermeasures. These computer codes include programs in one space dimension, and axisymmetric coordinates.

As a result of the investigation, specific design parameters, candidate materials and fields for further study have been identified.

SUMMARY

The concept of a locking material and the potential effectiveness of the locking material for possible use as a countermeasure to specified mine blasts have been investigated in this report. The effectiveness of the countermeasure has been demonstrated by the use of analytical methods and second order accurate computer codes. Computer codes have been developed to investigate and evaluate such a design that uses the countermeasures. These computer codes include programs in one space dimension, and axisymmetric coordinates.

As a result of the investigation, specific design parameters, candidate materials and fields for further study have been identified.

CONTENTS

1. INTRODUCTION

This report presents the results, to date, of investigations concerning the development of a countermeasure to mine blasts. In particular, the investigations have been conducted to develop computer simulation techniques that are capable of simulating the transient dynamic response of Locking materials[1,2] or locking material-structure combinations. These deveoloped techniques have been used to

(a) examine if a locking material shield has the potential of protecting a given structure from dynamic loads that have a time history similar to that of mine blasts, and

(b) provide a tool for designing the locking material shield-structure combination.

Terms such as foams, distended materials[3] or nonreactive porous solids[4], have been used to describe the locking materials. Typically, a locking material is characterized by a hydrostatic pressure-density curve similar to that shown in Figure 1.1. The model described in Figure 1.1 is an idealized behavior. In practice, a more realistic model may be necessary. A material, which follows the model shown in Figure 1.2 behaves like an elastic solid below a pressure p_E. For pressure $p > p_E$, the pore spaces collapse and the material locks at a density ρ_ℓ. The subsequent behavior of the material is that of an incompressible material. In practical shock interaction and attenuation calculations by numerical techniques, the model shown in Figure 1.1 is very often replaced by a pressure density relationship similar to those shown in Figures 1.2 or 1.3. In Figure 1.3, after reaching the locking density, the material is assumed to follow a pressure-density behavior of the corresponding solid. Furthermore, unloading will follow different paths as shown in the Figures 1.2 and 1.3. Such unloading paths are necessary to reflect the fact that a collapsed porous space can not be recovered. An exception to this rule is the behavior of graphite foam[3].

The theoretical foundation for expecting a locking material to be an effective peak stress attenuator or a countermeasure to mine blasts can be summarized as follows. Materials, that approximate a pressure-density behavior of Figures 1.1, 1.2 or 1.3, imply a large ratio of unloading or rarefaction wave velocity to the loading or shock velocity. The large ratio is the result of the fact that the velocity of the loading shockwave is related to the slope of a straight line connecting the initial and final states in the

pressure density diagram. The velocity of the unloading wave or rarefaction wave is related to the slope of the pressure-density curve for the solid at the locked state. The attenuation is caused by the unloading or rarefaction wave overtaking the loading shock wave because of the relatively higher velocity of the unloading waves. In practical situations, the effects of shear stresses and yielding need to be considered.

1.1 Candidate Materials

In principle, locking material can be produced from any parent solid material. The needed process of production requires the formation of a nonreactive porous solid of a density lower than that of the parent material. A commerical aluminum locking material MO-AL (Emerson and Cummings) has been available in the past. This is usually inhomogeneous. Homogeneous aluminum locking material can be produced by techniques[3] such as hot pressing of aluminum powders, cold pressing of aluminum powders followed by sintering or a repeated sequence of hot pressing that is followed by sintering of alumInum powders and the use of silica microballons. Commerically, graphite locking materials are available from companies such as National Carbon Company. Of course, a very common locking material of comparatively low threshold pressure capability that is easily available is the styro-foam. Depending on the environment and the peak stresses that need to be attenuated, different types of locking materials can be chosen or designed for a particular application. For example, in the case of a tank that is subjected to mine blasts, a locking material made of steel may be an interesting possibility. In some cases, a combination of different locking materials or a sandwich construction may be more practical.

1.2 Theoretical Foundation

First, a locking material in a state of one dimensional strain along x-axis is considered. A pressure-density relationship as shown in Figure 1.4 has been assumed. Initially, stresses and velocities in the region $x \geq 0$, have been assumed to be equal to zero. At time $t = 0$, it is assumed that a stress $-\sigma_x = \sigma_0$ is applied at the left boundary. The left boundary is initially at $x = x_0 (t = 0) = 0$ (figure 1.5). In addition to the pressure density behavior, the behavior in shear is assumed to be elastic-plastic with the following yield condition.

$$(\sigma_1 - \sigma_2)^2 + (\sigma_2 - \sigma_3)^2 + (\sigma_3 - \sigma_1)^2 = 2Y^2 \qquad (1.1)$$

In this equation, σ_1, σ_2, σ_3 are the principal stresses and Y is the yield stress in simple tension. For the assumed one-dimensional strain conditions, a $\sigma_x - \rho$ relationship can be derived from the pressure-density relationship and the assumed yield condition. The resulting $\sigma_x - \rho$ relationship is illustrated in Figure 1.6. The slope of the $\sigma_x - \rho$ curve for $\rho \geq \rho_\ell$ is derived from the mechanical behavior of the solid that constitutes the parent material for the given locking material of initial density ρ_o. For example, ρ_o for an aluminum locking material can be in the range of 1.1 gms/c.c. to 2.3 gms/c.c. The value of ρ_ℓ is approximately equal to 2.7 gms/c.c. In practice, ρ_ℓ is usually slightly below the value of the solid density of the parent material.

For $t>0$, the applied stress at the left boundary results in two stress waves propagating in the positive x-direction. The first wave is an elastic forerunner that carries the stress discontinuity that corresponds to $\tilde{Y}$*. The second wave is a shock wave that carries the stress discontinuity that corresponds to the difference between σ_o and $\tilde{Y}$*. The shockwave velocity is denoted by $\dot{k}$. The following jump conditions are valid across the elastic forerunner and the shock wave.

$$\rho_0(\dot{k}_e - v_0) = \rho_e(\dot{k}_e - v_e) \qquad (1.2)$$

$$\tilde{Y} = -\rho_e(\dot{k}_e - v_e)\, v_e + \rho_o(\dot{k}_e - v_o)\, v_o \qquad (1.3)$$

$$\rho_\ell(\dot{k}_\ell - v_\ell) = \rho_e(\dot{k}_\ell - v_e) \qquad (1.4)$$

$$\bar{\sigma} - \tilde{Y} = -\rho_\ell(\dot{k}_\ell - v_\ell)\, v_\ell + \rho_e(\dot{k}_\ell - v_e)\, v_e \qquad (1.5)$$

In these equations, v_e and v_ℓ are the particle velocities ahead of the elastic forerunner wave and behind the forerunner wave respectively. The velocity of elastic forerunner wave itself is equal to $\dot{k}_e$ and v_ℓ is the particle velocity behind the shock wave. From initial conditions, $v_o = 0$. From equations (1.4) and (1.5) the shock wave velocity $\dot{k}_\ell$ is given by the following equation.

$$\dot{k}_\ell = v_e + \sqrt{\frac{\bar{\sigma} \cdot \tilde{Y}}{\rho_e(1 - \frac{\rho_e}{\rho_\ell})}}$$

---

* $\tilde{Y} = \left(\frac{K}{2G} + \frac{2}{3}\right) Y$

Usually, v_e is very small and

$$\rho_e \simeq \rho_o$$

Then

$$\dot{k}_\ell = \sqrt{\frac{\bar{\sigma} - Y}{\rho_o(1 - \frac{\rho_o}{\rho_\ell})}} \quad .$$

This is the velocity of the loading shock wave in the locking material. For example, for aluminum locking material of initial density $\rho_o = 1.5$ gms/c.c., $\rho_\ell = 2.7$ gms/c.c., Y = 37,500 psi (258.6 mpa) and σ_o = 125,000 psi (862 mpa) the velocity of the loading shock wave is 3354 feet per second (1022 m/sec) which is approximately 20% of the longitudinal elastic wave velocity of the solid aluminium. These examples qualitatively illustrate the slow loading velocities in a locking material of low initial density. However, it is to be noted that the shock wave velocity in a solid is slower than the corresponding longitudinal elastic wave velocity. Even then, the shock wave velocity can be shown to be slower in locking materials than in the corresponding solid.

1.3 Experimental Background

In the past, experimental investigations have been conducted[3] on several locking materials. In these investigations, metals, plastics, graphite and ceramics have been used as parent materials to produce locking materials. Experiments have been conducted by using light gas guns and flyer plates. In these experiments, attempts have been made to simulate conditions of one dimensional strain. From the point of view of the present study, a significant result from these studies concerns a comparison of the shock wave velocities in locking materials with the corresponding wave velocities in solid materials.

In most of these studies, a two wave pattern has been observed in locking materials and solids. In locking materials, a forerunner wave carries stresses in the material before the phase transition from the initial density ρ_0 to the locked density ρ_ℓ. The second slow wave corresponds to the shock wave that was discussed in the previous section. This shock wave carries stresses that exceed the stresses necessary for phase transition. Solid materials also exhibit a two wave pattern. In this case, the stresses carried by the forerunner wave correspond to the yield limit and the elastic behavior of

the solid before yield. This forerunner wave travels at a velocity corresponding to the longitudinal elastic wave velocity in the isotropic solid. The second wave carries stresses that exceed the elastic limit. The experiments confirm the fact that this second wave in the solid is much faster than the second shock wave in the locking material. For example, in aluminum locking materials of initial density ρ_0 = 2.1 gms/c.c., the second shock wave velocity varied from 0.7 to 1.29 mm/μsec. The second wave velocity, in the corresponding solid was in the range of 4.62 mm/μsec. Similarly, the first wave velocities in the locking materials were smaller than the first wave velocities in the corresponding solid. The first wave velocities, in aluminum locking materials of initial density ρ_0 = 2.1 gms/c.c., varied in the range 1.6 mm/μsec to 2.0 mm/μsec. The corresponding first wave in the solid travelled with a velocity of 6.11 mm/μsec.

The theoretical foundation and the results of the experimental studies confirm the potential benefits that can be derived from locking materials when they are used as protective structures.

2. RESEARCH PLAN

2.1 Problems Associated With Engineering Design

In the point of view of engineering designs, the results of this project should provide tools to design a countermeasure or a protective structure for the mine blasts that will be specified. In this report, however, the protective structure for mine blasts is assumed to be made of a locking material. Specifically, such a design involves the selection of a parent material from which the locking material is produced, the thickness of the protective structure, other geometrical parameters and methods of joining the countermeasure to the structure. In addition, the selection of an initial density for the locking material and the specification of the desired microstructure constitute important aspects of the design. The selected initial density, the specified production technique and the resulting microstructure, usually determine the range of pressures at which the phase transition takes place from the initial density to the locked density. The microstructure is also responsible for the elastic-plastic stress-strain behavior and the associated yield conditions.

An essen 'al design tool for the selection of the various design parameters, is a comp 'er sim .tion that is capable of providing the transient dynamic response of the

locking material or the locking material and structure combinations. The specified mine blasts and the various design parameters can be supplied as an input to the resulting computer program. The output can be obtained as deformations and stresses at various locations as a function of time. The output data can then be used

(a) to check if the selected design parameters provide the desired margin of safety for various failure modes,

(b) to iterate or to modify the design parameters and

(c) to establish the damage tolerance and reliability of the design.

The primary objective of the reported investigations is to develop such computer simulations and the resulting computer programs. To date, most of the reported investigations have been restricted to one space dimension and time. The results have been mainly used to simulate the experimental results. The programs have not been used to study the effectiveness of the locking material as a countermeasure to resist mine blasts. A study of the transient dynamic response of a locking material that involved two space dimensions and time has been reported by the author[4]. This study described the impact of compactible plates under axisymmetric conditions. The constitutive relationship that was used for the compactible plate is very specialized and cannot be easily generalized for the locking materials of concern here. The one dimensional analysis and the compactible plate analysis have used the finite difference technique developed by Von Neuman,[26, 30] and Wilkins[31]. Certain difficulties were encountered in the application of the Von Neuman's approach to locking materials.

(1) Very small time steps were needed to account for the phase transition from the initial density to the locked density.

(2) An accurate computer simulation of the precursor wave was very difficult.

(3) Computational efficiency and the level of accuracy decreased when two or more space dimensions were considered. Similar problems were encountered in considering multiple reflections.

Other investigators[3,4] also experienced similar difficulties in applying the Von Neumann's technique to the study of the dynamic response of locking materials and phase

transition. In order to reduce these difficulties and to develop the needed computer simulation techniques for transient dynamic response of locking materials, the following research plan was adapted.

(1) The first step was to prepare a state-of-the-art review of finite difference methods for the numerical solution of hyperbolic differential equations.

(2) The second step was to select a computationally efficient and accurate finite difference method.

(3) The selected second order accurate method was then applied to study the transient response of locking material structures under the conditions of one dimensional strain. The purpose of the analysis was to demonstrate the capabiltiy of locking material as a countermeasure to mine blasts.

(4) Then, a computer simulation of locking material was developed under conditions of axisymmetry and finite deformations.

3. STATE-OF-THE-ART

The field of the analysis of the transient dynamic response of elastic-plastic-locking materials is in the general field that is concerned with seeking solutions to nonlinear hyperbolic differential equations. For both linear and nonlinear differential equations, that are encountered in the field of solid mechanics, very few analytical solutions have been obtained. As a consequence, alternative methods of solutions have been sought for many practical problems of solid mechanics. Integral tranform techniques have been very effective tools in solving linear elastodynamic problems[5-7]. Primarily, integral transforms, such as Laplace tranforms, have been used to remove time as an independent variable. This effectively reduces the equation to an elliptic type. After the solutions have been obtained to the reduced equation, in tranformed variables, the next operation is to obtain the inverse tranform to return the solution to the time domain. One of the particularly successful techniques of obtaining the inverse transforms for elastodynamic problems, is the Cagniard-deHoop technique[8]. Basically, this method involves the modification of the contour of integrations that are encountered in the process of obtaining inverse transforms, in such a way that the integrals are rendered to a form with known solutions. This technique has been successfully applied to many solid mechanics problems[9-22].

These tranform techniques have limitations when applied to nonlinear problems and

structures with finite boundaries. For this class of problems, other numerical methods are necessary. Numerical methods that use the method of characteristics, have been primarily restricted to the class of one space dimensional problems. Butler[23] and Clifton[24] have reported the applications to two space dimensional problems. Most of the developments in the last two decades have used finite difference and finite element methods to solve the transient dynamic response problems in solids.

3.1 Finite Difference Methods

The research activity of the sixties and seventies has proved that the finite element methods are superior to other numerical methods in solving elastostatic problems. However, the same superiority does not apply to linear or nonlinear transient dynamic response problems in solids. In fact, the finite difference methods offer a viable choice to the solution of transient dynamic response problems. It has been shown[25] that, for selected problems, finite difference methods provide better accuracy and computational efficiency when compared with the solutions obtained by using finite element methods. The rest of this review of the state-of-the-art is restricted to finite difference methods and their application to the study of the linear and nonlinear transient dynamic response problems in solids.

Early work in the field of the application of the finite difference methods to transient dynamic response of solids, consisted of the application of a finite difference scheme developed by Von Neumann[26] for use in hydrodynamics. The Von Neumann's scheme is an explicit finite difference approximation of the time derivatives and is often classified as "Leap Frog" scheme[27]. A classic paper in this field is by Wilkins[28] to solve two and three-dimensional transient[29] elastodynamic problems. Wilkins has also considered ideal plasticity and large deformation effects in his studies.

In Wilkin's approach, as is done in all leap frog schemes, the dependent variables are staggered in space and time to satisfy the stability requirements and maintain second order of accuracy. This results in the calculation of only one set of field variables at any particular mesh point. This means that only stresses or velocities are computed at a selected mesh point. Furthermore, such a staggered scheme sometimes results in computationally induced oscillations[30]. These computationally induced oscillations can be minimized by using an artificial viscosity[26]. However, the use of the artificial viscosity results in a finite difference scheme that is not optimally stable[30]. The time steps are often reduced by a factor of three in two-dimensional problems[28,29].

Variations of Wilkins' approach[31-36] appear throughout the literature in the field of the study of transient elastodynamic problems. Clifton[24] has proposed a different approach to the problem. He has extended the difference scheme developed by Butler[23], for hydrodynamics, to study two-dimensional elastodynamic problems. This finite difference scheme has been developed by formulating integration procedures along bicharacteristics. The resulting procedure is an explicit finite difference scheme. Unlike the leap frog scheme, all the variables are calculated at all mesh points.

Lax and Wendroff[37] have developed a second order accurate scheme for hydrodynamic problems. In this scheme, all the dependent variables are calculated at all mesh points. At interior points Clifton's scheme and Lax-Wendroff's scheme are identical. Both these schemes, however, are not optimally stable, in the sense of Courant, Friedrich and Levy, for more than one space dimension[38]. This leads to computational procedures that are less than optimally efficient. Also the Lax-Wendroff schemes involve computation of squares of certain matrices and result in a complicated algorithm. Smith[39] has applied the Lax-Wendroff procedures and the early time splitting procedures of Strang[40] to two-dimensional problems. Smith's work is concerned with the comparison of the relative efficiency of the schemes and is not a complete initial boundary value problem.

However, an improved version of Lax-Wendroff's scheme, that has the potential of providing an improved computational efficiency and accuracy, can be applied to both linear and nonlinear transient dynamic response problems in solid mechanics. The improvement can be incorporated in three different areas. The first improvement is in the modification of the scheme to make it optimally stable[40]. This is due to Strang[40,41] and somewhat similar to that used by Smith. The second improvement is to improve the computational efficiency by providing second order accuracy at every other time step. This improvement follows the developments of Gottlieb[38], Gourlay[42], Morris[42] and Mitchell[43]. The third improvement is in the incorporation of McCormack's[44] two step procedure. This third improvement results in programming simplicity and eliminates the need for squaring the matrices that is needed in Lax-Wendroff or Strang's procedures. This improvement is very useful in solving nonlinear problems.

An improvement in the implementation of the finite difference schemes is the concept of point condition codes[25]. Attempts at improvement of osillations, overshoots and smearing of contact discontinuities are also possible[45-51].

4. ANALYSIS UNDER CONDITIONS OF ONE-DIMENSIONAL STRAIN

4.1 Development of the Procedure

The proposed second order accurate method of analyzing the behavior of the locking material has received little attention when applied to solid mechanics problems. The efficiency and the resulting accuracy of the method have been studied as a part of another sponsored research project at Georgia Tech. In this project, one and two-dimensional problems of transient dynamic analysis have been investigated. At present, nonlinear problems have been studied. In the previous analyses, the nonlinear behavior has not been studied.

In this section, the proposed second order accurate difference scheme has been applied to the transient dynamic response of locking materials. The application is restricted to one-dimensional strain in the x-direction. The numerical results are presented for the specific cases of loading for aluminum locking materials. This study is undertaken for the following reasons.

(1) one-dimensional problem is relatively simple

(2) the analysis provides an understanding of how the proposed second order accurate difference schemes can handle the phase transition

(3) the effect of different initial densities for the various locking materials can be qualitatively understood with regard to a one-dimensional analysis.

(4) The method of analysis for one-dimensional problems would indicate the possible areas of difficulties that may be encountered when extended to two and three-dimensional problems of transient dynamic analysis of locking materials.

The one-dimensional equations of motion have been written in Lagrangian coordinates. The initial positions of the body have also been selected as the Lagrangian coordinates. Large elastic-plastic deformations of the locking material have been considered. The resulting equations are as follows:

$$\frac{\partial}{\partial t}\{\underset{\sim}{u}\} = A(\rho)\ \frac{\partial}{\partial x}\{\underset{\sim}{u}\} \tag{4.1}$$

where

$$\{\underset{\sim}{u}\}^T = \left\{v(x,t),\ \rho(x,t), \sigma_x(x,t), \sigma_y(x,t)\right\}^T \tag{4.2}$$

and

$$\left[A(\rho)\right] = \begin{bmatrix} 0 & 0 & \rho^{-1} & 0 \\ -\rho & 0 & 0 & 0 \\ \rho f'(\rho) + \frac{4G}{3} & 0 & 0 & 0 \\ \rho f'(\rho) - \frac{2G}{3} & 0 & 0 & 0 \end{bmatrix} . \qquad (4.3)$$

In these equations, it has been assumed that the stress tensor can be separated into hydrostatic pressure and stress deviators. The hydrostatic pressure has been assumed to be related to the changes in density and follow a locking behavior as shown in Figure 1.3. The stress deviators are assumed to follow an elastic-ideal plastic behavior with Von Mises' yield condition.

All the assumptions of the preceding paragraph are approximations. However, these approximations have been used, in the past, to express the mechanical behavior of locking materials[3,4,52] and other solids[52] at very high stresses. On the basis of experimental results, the approximations have been found to be reasonable[52]. In the absence of any available constitutive relationships on the basis of second Piola-Kirchhoff stresses and Green-Lagrange strains, this paper has considered similar approximations. The constitutive relationships have been written in terms of Cauchy stresses, particle velocity gradients and density. Then,

$$\sigma_x = -p + S_x \qquad (4.4)$$

$$\sigma_y = -p + S_y \qquad (4.5)$$

and

$$\left.\begin{array}{lll} p = f_1(\rho) & \rho_o < \rho < \rho_1 \\ p = f_2(\rho) & \rho_1 < \rho < \rho_\ell \\ p = f_3(\rho) & \rho_\ell < \rho \end{array}\right\} . \qquad (4.6)$$

The quantities f_1, f_2 and f_3 are as follows (Figure 1.3):

$$f_1(\rho) = P_1 \frac{\rho_1}{\rho_o}\left(\frac{\rho_o-\rho}{\rho_o-\rho_1}\right)\left[1 + b\left(\frac{\rho_o}{\rho}\right)\left(\frac{\rho_1-\rho}{\rho_o-\rho_1}\right)\right]$$

$$f_2(\rho) = P_1 + \frac{K}{R}\left[\left(\frac{\rho}{\rho_1}\right)^R - 1\right]$$

$$f_3(\rho) = A(\rho/\rho_G - 1) + B(\rho/\rho_G - 1)^2 \qquad (4.7)$$

Similarly,

$$\dot{S}_x = -2\dot{S}y = -2\dot{S}_z = -\frac{4}{3} G \frac{\dot{\rho}}{\rho} \qquad (4.8)$$

with the yield condition

$$S_x^2 + 2Sy^2 - \frac{2}{3} Y^2 \leq 0. \qquad (4.9)$$

4.2 Numerical Analysis

A numerical integration of the hyperbolic partial differential equation (4.1) by a procedure similar to that of Lax requires that the field variables $\{\underset{\sim}{u}\}$ at $t + \Delta t$ should be calcualted from a knowledge of the field variables $\{\underset{\sim}{u}\}$ and its spatial derivatives at t. To a second order accuracy,

$$\{\underset{\sim}{u}\}^{t+\Delta t} = \{\underset{\sim}{u}\}^t + \left\{\frac{\partial \underset{\sim}{u}}{\partial t}\right\}^t \Delta t + \left\{\frac{\partial^2 \underset{\sim}{u}}{\partial t^2}\right\}^t \frac{\Delta t^2}{2} + O(\Delta t)^3 . \qquad (4.10)$$

The differential equation (4.1) can be used to express the quantities $\partial \underset{\sim}{u}/\partial t$ and $\partial^2 \underset{\sim}{u}/\partial t^2$ in terms of the spatial derivatives of $\{\underset{\sim}{u}\}$. Then,

$$\{\underset{\sim}{u}\}^{t+\Delta t} = \{\underset{\sim}{u}\}^t + [A(\rho)]\left\{\frac{\partial \underset{\sim}{u}}{\partial x}\right\}^t + [A(\rho)]^2\left\{\frac{\partial^2 \underset{\sim}{u}}{\partial x^2}\right\}^t \frac{\Delta t^2}{2}$$

$$+ [A(\rho)]\left[\frac{\partial A}{\partial x}\right]\left\{\frac{\partial \underset{\sim}{u}}{\partial x}\right\}^t \frac{\Delta t^2}{2} + \left[\frac{\partial A}{\partial t}\right]\left\{\frac{\partial \underset{\sim}{u}}{\partial x}\right\}^t \frac{\Delta t^2}{2} . \qquad (4.11)$$

The equation (4.11) is very complicated. It involves $[A(\rho)]^2$ and multiples of first and second partial derivatives of $\{ \underset{\sim}{u} \}$ with respect to x. This equation can be considerably simplified by using a two step approximation due to McCormack, Richtmyer or Gottlieb. For example, McCormack two step formulation is as follows.

$$\{ \underset{\sim}{u} \}^{*} = \{ \underset{\sim}{u} \}^{t} + \left\{ \frac{\partial \underset{\sim}{u}}{\partial t} \right\}^{t} \Delta t$$

$$\{ \underset{\sim}{u} \}^{t+\Delta t} = \frac{1}{2}\left(\{ \underset{\sim}{u} \} + \{ \underset{\sim}{u}^{*} \} \right) + \frac{\Delta t}{2} \left\{ \frac{\partial \underset{\sim}{u}^{*}}{\partial t} \right\} \qquad (4.12)$$

It is easy to verify the accuracy of (4.12) by expansion. Now, the time derivatives on the right hand sides of (4.12) are replaced by spatial derivatives. Thus,

$$\{ \underset{\sim}{u} \}^{*} = \{ \underset{\sim}{u} \}^{t} + [A(\rho)] \frac{\partial \underset{\sim}{u}}{\partial x}^{t} \Delta t.$$

$$\{ \underset{\sim}{u} \}^{t+\Delta t} = \frac{1}{2}\left(\{ \underset{\sim}{u} \} + \{ \underset{\sim}{u} \}^{*} \right) + \frac{\Delta t}{2} [A]^{*} \frac{\partial \underset{\sim}{u}^{*}}{\partial x} . \qquad (4.13)$$

It is to be noted that $[A(\rho)]^{*}$ and $\partial y/\partial x^{*}$ are to be evaluated by using the star values of the field variables. Also, it can be seen that the formulation described in the equations (4.13) is much simpler than the formulation described in (4.11). To complete the finite difference formulation, the spatial derivatives of $\{ \underset{\sim}{u} \}$ and $\{ \underset{\sim}{u} \}^{*}$ are expressed in terms of their spatial finite difference approximations. A central, forward or backward difference is used depending on whether the point under consideration is an interior point, left boundary point or right boundary point.

4.3 Stability Requirements

The equations (4.13) can be written in the form of finite difference operators. Then,

$$L^{*} = [I] + k[A]\Delta_x$$

$$L_1 = \frac{1}{2}\left([I] + k[A]\Delta_x \right) . \qquad (4.14)$$

In these equations, Δx represents the spatial finite difference approximations. The quantity I is the identity operator and Δt has been replaced by k. Then,

$$\left\{ \underset{\sim}{u} \right\}^{t + \Delta t} = \left(\frac{I}{2} + L_1 L^* \right) \left\{ \underset{\sim}{u} \right\}^{t} \quad . \tag{4.15}$$

The operators I, L_1 and L^*, operating on $\left\{ \underset{\sim}{u} \right\}^{t}$ in the manner shown in equation (4.15) change $\left\{ \underset{\sim}{u} \right\}^{t}$ to $\left\{ \underset{\sim}{u} \right\}^{t + \Delta t}$. This is an explicit scheme and is subject to the usual restrictions on $k = \Delta t$ to maintain the stability of the computational scheme. In particular, it can be shown that $\Delta t \ll \Delta x/c$ where c is the fastest of the local elastic wave velocities.

4.4 Plasticity Effects and Yield Conditions

The numerical method that has been used in this paper is an explicit method. The field variables at $t + \Delta t$ depend only on the field variables, at time t. The particle velocities and strains at $t + \Delta t$ can be computed from the current field variables at t. The stresses computed at $t + \Delta t$ may violate the yield condition (4.9). However, these stresses can be adjusted along appropriate normals to the yield surface back to the yield surface[52]. The already calculated velocities and strains that depend only on the field variables at t remain unchanged. The only regions where iterative calculations are needed are at the boundaries.

4.5 Discussion of Results

In order to achieve the same accuracy as a first order accurate method, a time step equal to the square root of Δt that is used in the first order method is needed. The quantity Δt is usually less than one and hence the second order accurate method uses a larger time step. Hence, a larger Δt can be chosen to obtain the same order of accuracy as a first order method. This leads to a smaller number of the finite difference cells and increased computational efficiency. The developed computer program has been used to examine the efficiency of locking materials in attenuating stresses and protecting structures. In this analysis, specified items include the peak impact stress and the unloading pattern of the stress wave impinging on the locking materials. The locking

density ρ_ℓ is usually fixed for a given locking material. The results of the numerical analysis can be used to explain the peak stress and the stress distribution for various times after impact and unloading at the boundary.

In the numerical example, aluminum locking materials have been selected. Some of the properties of aluminum locking materials have been extensively investigated[3]. A pressure density relationship as shown in Figure 1.3 has been assumed. The locking density ρ_ℓ is equal to the 2.72 gms/c.c. Various initial densities have been considered. Results have been presented for ρ_o = 1.39 and 2.1 gms/c.c here. There are three distinct branches of the pressure-density relationship. Equations for these branches are the same as in equations (4.6) and (4.7).

The quantity ρ_G is the intersection of the $p - \rho$ curve with ρ axis as shown in Figure 1.3. The appropriate constants are selected from reference 3. For all $\rho > \rho_\ell$, the unloading is assumed to follow the slope of the solid $p - \rho$ curve as shown in Figure 1.3.

Two types of loading have been considered. The first type of loading consists of a step loading followed by step unloading. It has been assumed that a peak compressive stress of σ_o is applied at time t = 0 to the left boundary of the slab of a locking material. For purposes of illustration, a value of $-\sigma_o$ = 100,000 psi (689.5 MPa) has been assumed. The applied stress is reduced to zero by step unloading at time $\bar{t}$ = 0.2 μsec. This loading pattern is illustrated in Figure 4.1 and will be called loading pattern 'a'. The second type of loading consists of a step loading of a compressive stress of magnitude $-\sigma_o$ at t = 0 followed by an exponential unloading at the left boundary. For purposes of illustration, $-\sigma_0$ has been assumed to be equal to 100,000 psi (689.5 MPa). The applied stress is assumed to be maintained at $\sigma = -\sigma_0$ for a duration of 0.02 μsec. Then the exponential decay of the applied load at the left boundary decreases the magnitude of σ_0 to .05 σ_0 at 0.2 μsecs. This unloading pattern is illustrated in Figure 4.2 and will be called loading 'b'.

First, a solid material slab of initial thickness 0.5 inches (12.7 mm) has been considered. The thickness has been divided into 100 cells. In this case the solid density is ρ_ℓ = 2.72 gms/c.c. The transient response of this slab to the loading pattern 'a' has been studied by using the developed computer program and the results are illustrated in Figure 4.3. This figure is a plot of the stress σ_x as a function of the thickness at two different instants of time t = 0.21 μsecs and t = 0.68 μsecs. As seen in the figure, the stress at a distance of 0.14 inch (3.6 mm) from the initial left boundary is still approximately 100,000 psi (689.5 MPa). This is equal to the applied peak stress. No significant attenuation has taken place during the travel of the stress wave through the

thickness equal to 0.14 inch (3.6 mm).

Next, a locking material of initial density ρ_o = 2.1 gms/c.c. and locking density ρ_ℓ = 2.72 gms. c.c. has been considered. The thickness and division into cells are identical to those for the solid. The transient response to the loading pattern 'a' has been computed and illustrated in Figure 4.4. The stress distribution as a function of the distance from the left boundary has been illustrated for t = 0.13 μsec, 0.54 μsec, 1.15 μsec, and 2.22 μsec. It can be seen that the peak stress has reduced by approximately 35% over a distance of 0.09 inch (2.3 mm) from the left boundary. In this figure, the elastic forerunner wave can also be seen. Similar stress distributions are observed for locking materials of initial density ρ_o = 1.818 gms/c.c., 1.604 gms/c.c. and 1.39 gms/c.c. If these locking materials are considered as countermeasures in front of a given structure, the peak impact stress has been reduced by an amount as much as 50% when the shock wave has propagated a distance of 0.013 inch (0.33 mm) (Figure 4.5). It can also be observed that the locking material of lower initial density has the potential of attenuating the impact peak stress by a larger percentage when compared with the locking material of higher initial density.

As a next step, the loading pattern 'b' has been considered. The results of the study of transient response through a solid has been illustrated in Figure 4.6. The results are similar to those for the loading pattern 'a'. The peak impact stress has not attenuated during the passage of the stress wave over a distance of 0.15 inch (3.8 mm). Similar stress distribution for loading pattern 'b' has been illustrated in Figures 4.7 and 4.8 for different locking materials of initial density ρ_o = 2.1 gms/c.c. and 1.39 gms/c.c. The Figure 4.7 is for a locking material with initial density 2.1 gms/c.c. Over a shock wave traverse of .045 inch the peak stress has been reduced by 60%. However, the locking material with initial density of 1.39 gms/c.c. can attenuate the peak stress by almost 90%, during the shock traverse of 0.05 inch (1.3 mm). This is illustrated in Figure 4.8. The unloading waves and the elastic forerunners can be identified in all these figures. In Figure 4.9, the effect of the plasticity on the transient dynamic response is shown. A yield stress of 80,000 psi is assumed for purposes of illustration.

5. ELASTIC - PLASTIC - LOCKING MATERIALS UNDER CONDITIONS OF AXISYMMETRY

5.1 Introduction

In this section, the numerical scheme that has been discussed in Sections 3 and 4

has been modified and applied to study the transient dynamic response of elastic-plastic locking materials under conditions of axisymmetry. A cylindrical polar coordinate system r, θ, z has been used. Initial positions of various material points have been used as Lagrangian coordinates. The problem has been formulated as a finite deformation problem with Cauchy stresses that are defined in a deformed coordinate system. In order to represent the equations in a form that is suitable for the use of Gottlieb[36]-MacCormack[44]-Strang[40,41] type of scheme, the constitutive relationships have been used in a rate form. The Jaumann stress[53] rate (or the corotational stress rate) has been used to satisfy the principle of objectivity.

5.2 Governing Equations

The governing equations are then written as follows.

Kinematic equations:

$$\dot{z} = w \tag{5.1}$$

$$\dot{r} = u \tag{5.2}$$

Equations of motion:

$$\dot{w} = \frac{1}{\rho}\frac{\partial \sigma_{zz}}{\partial z} + \frac{1}{\rho}\frac{\partial \tau_{zr}}{\partial r} + \frac{1}{\rho}\frac{\tau_{zr}}{r} \tag{5.3}$$

$$\dot{u} = \frac{1}{\rho}\frac{\partial \tau_{zr}}{\partial z} + \frac{1}{\rho}\frac{\partial \sigma_{rr}}{\partial r} + \frac{1}{\rho}\frac{\sigma_{rr}-\sigma_{\theta\theta}}{r} \tag{5.4}$$

Constitutive equations:

$$\dot{\sigma}_{zz} = (\rho\frac{dp}{d\rho} + \frac{4}{3}G)\frac{\partial w}{\partial z} + (\rho\frac{dp}{d\rho} - \frac{2}{3}G)\frac{\partial u}{\partial r} + (\rho\frac{dp}{d\rho} - \frac{2}{3}G)\frac{u}{r} + \tau_{zr}(\frac{\partial w}{\partial r} - \frac{\partial u}{\partial z}) \tag{5.5}$$

$$\dot{\sigma}_{rr} = (\rho\frac{dp}{d\rho} - \frac{2}{3}G)\frac{\partial w}{\partial z} + (\rho\frac{dp}{d\rho} + \frac{4}{3}G)\frac{\partial u}{\partial r} + (\rho\frac{dp}{d\rho} - \frac{2}{3}G)\frac{u}{r} + \tau_{zr}(\frac{\partial u}{\partial z} - \frac{\partial w}{\partial r}) \tag{5.6}$$

$$\dot{\sigma}_{\theta\theta} = (\rho\frac{dp}{d\rho} - \frac{2}{3}G)\frac{\partial w}{\partial z} + (\rho\frac{dp}{d\rho} - \frac{2}{3}G)\frac{\partial u}{\partial r} + (\rho\frac{dp}{d\rho} + \frac{4}{3}G)\frac{u}{r} \tag{5.7}$$

$$\dot{\tau}_{zr} = G\frac{\partial u}{\partial z} + G\frac{\partial w}{\partial r} + \frac{1}{2}(\sigma_{zz} - \sigma_{rr})(\frac{\partial u}{\partial z} - \frac{\partial w}{\partial r}) \tag{5.8}$$

Continuity equation:

$$\dot{\rho} = -\rho\frac{\partial w}{\partial z} - \rho\frac{\partial u}{\partial r} - \rho\frac{u}{r} \tag{5.9}$$

It has been assumed that

$$p = p(\rho) \tag{5.10}$$

follows the equations similar to (4.6) that represent a locking behavior. A Von Mises yield condition and ideal plasticity have been assumed.

$$(\sigma_{zz} + p)^2 + (\sigma_{rr} + p)^2 + (\sigma_{\theta\theta} + p)^2 + 2\tau_{zr}^2 \leq \frac{2}{3}Y^2 \tag{5.11}$$

The notation used in the equations are as follows:

z,r	current positions of the coordinate
w	velocity in z-direction
u	velocity in r-direction
σ_{zz}	normal stress in z-direction
σ_{rr}	normal stress in r-direction
$\sigma_{\theta\theta}$	normal stress in -direction
τ_{zr}	shear stress
ρ	density
p	hydrostatic pressure
G	modulus of rigidity
Y	yield stress in simple tension
L	length, in the z-direction
R	radius of the structure

The equations (5.1) to (5.9) can be rewritten in the following form

$$\{\dot{u}\} = [A]\{u\}_{,z} + [B]\{u\}_{,r} + [C]\{u\} \tag{5.12}$$

where

$$\{u\}^T = \{z, r, w, u, \sigma_{zz}, \sigma_{rr}, \sigma_{\theta\theta}, \tau_{zr}, p\}^T \quad .$$

The matrices $[A]$,$[B]$ and $[C]$ are not constants in the finite deformation problem of elastic-plastic-locking materials. Specifically

$$[A] = \begin{bmatrix} 0 & 0 & 0 & 0 & 0 & 0 & 0 & 0 & 0 \\ 0 & 0 & 0 & 0 & 0 & 0 & 0 & 0 & 0 \\ 0 & 0 & 0 & 0 & 1/\rho & 0 & 0 & 0 & 0 \\ 0 & 0 & 0 & 0 & 0 & 0 & 0 & 1/\rho & 0 \\ 0 & 0 & \frac{dp}{d\rho} + \frac{4G}{3} & -\tau_{zr} & 0 & 0 & 0 & 0 & 0 \\ 0 & 0 & \frac{dp}{d\rho} - \frac{2G}{3} & \tau_{zr} & 0 & 0 & 0 & 0 & 0 \\ 0 & 0 & \frac{dp}{d\rho} - \frac{2G}{3} & 0 & 0 & 0 & 0 & 0 & 0 \\ 0 & 0 & 0 & G+\frac{1}{2}(\sigma_{zz} - \sigma_{rr}) & 0 & 0 & 0 & 0 & 0 \\ 0 & 0 & -\rho & 0 & 0 & 0 & 0 & 0 & 0 \end{bmatrix} \tag{5.13}$$

$$[B] = \begin{bmatrix} 0 & 0 & 0 & 0 & 0 & 0 & 0 & 0 & 0 \\ 0 & 0 & 0 & 0 & 0 & 0 & 0 & 0 & 0 \\ 0 & 0 & 0 & 0 & 0 & 0 & 0 & 1/\rho & 0 \\ 0 & 0 & 0 & 0 & 0 & 1/\rho & 0 & 0 & 0 \\ 0 & 0 & \tau_{zr} & \rho\frac{dp}{d\rho} - \frac{2G}{3} & 0 & 0 & 0 & 0 & 0 \\ 0 & 0 & -\tau_{zr} & \rho\frac{dp}{d\rho} + \frac{4G}{3} & 0 & 0 & 0 & 0 & 0 \\ 0 & 0 & 0 & \rho\frac{dp}{d\rho} - \frac{2G}{3} & 0 & 0 & 0 & 0 & 0 \\ 0 & 0 & G - \frac{1}{2}(\sigma_{zz} - \sigma_{rr}) & 0 & 0 & 0 & 0 & 0 & 0 \\ 0 & 0 & 0 & -\rho & 0 & 0 & 0 & 0 & 0 \end{bmatrix} \tag{5.14}$$

and

$$[C] = \begin{bmatrix} 0 & 0 & 1 & 0 & 0 & 0 & 0 & 0 & 0 \\ 0 & 0 & 0 & 1 & 0 & 0 & 0 & 0 & 0 \\ 0 & 0 & 0 & 0 & 0 & 0 & 0 & 1/\rho r & 0 \\ 0 & 0 & 0 & 0 & 0 & 1/\rho r & -1/\rho r & 0 & 0 \\ 0 & 0 & 0 & (\rho\frac{dp}{d\rho} - \frac{2G}{3})/r & 0 & 0 & 0 & 0 & 0 \\ 0 & 0 & 0 & (\rho\frac{dp}{d\rho} - \frac{2G}{3})/r & 0 & 0 & 0 & 0 & 0 \\ 0 & 0 & 0 & (\rho\frac{dp}{d\rho} + \frac{4G}{3})/r & 0 & 0 & 0 & 0 & 0 \\ 0 & 0 & 0 & 0 & 0 & 0 & 0 & 0 & 0 \\ 0 & 0 & 0 & -\rho/r & 0 & 0 & 0 & 0 & 0 \end{bmatrix} . \quad (5.15)$$

5.3 Numerical Method

For the hyperbolic differential equation (5.12), the Lax-Wendroff second order operator can be written as follows.

$$\{u\}^{t+\Delta t} = L_{zr}\{u\}^{t} \quad (5.16)$$

where

$$L_{zr} = [I] + \Delta t([A]\Delta_z + [B]\Delta_r + [C])$$
$$+ \frac{\Delta t^2}{2}\Big\{[A]^2\Delta_{zz} + [B]^2\Delta_{rr} + ([A][B] + [B][A])\Delta_{rz}$$
$$+ [A][A]_{,u}\Delta_z\Delta_z + [B][A]_{,u}\Delta_r\Delta_z$$
$$+ [A]_{,u}[A]\Delta_z\Delta_z + [A]_{,u}[B]\Delta_r\Delta_z + [A]_{,u}[C]\Delta_o\Delta_z$$
$$+ ([A][C] + [C][A])\Delta_z$$

$$+ [A][B]_{,u}\,\Delta_z\,\Delta_t + [B][B]_{,u}\,\Delta_t\,\Delta_t$$

$$+ [B]_{,u}[A]\,\Delta_z\,\Delta_r + [B]_{,u}[B]\,\Delta_r\,\Delta_r$$

$$+ [B]_{,u}[C]\,\Delta_o\,\Delta_r + ([B][C] + [C][B])\,\Delta_r$$

$$+ [A][C]_{,u}\,\Delta_z\,\Delta_o + [B][C]_{,u}\,\Delta_r\,\Delta_o + [C]_{,u}[A]\,\Delta_z\,\Delta_o$$

$$+ [C]_{,u}[B]\,\Delta_r\,\Delta_o + [C]_{,u}[C]\Delta_o\,\Delta_o + [C]^2\Big\}\Delta_o \quad . \tag{5.17}$$

In this equation, the quantities

$$\begin{aligned}
\Delta_z\{u\} &\approx \frac{\partial}{\partial z}\{u\},\\
\Delta_r\{u\} &\approx \frac{\partial}{\partial r}\{u\},\\
\Delta_o\{u\} &\approx \{u\},\\
\Delta_{zz}\{u\} &\approx \frac{\partial^2}{\partial z^2}\{u\},\\
\Delta_{rr}\{u\} &\approx \frac{\partial^2}{\partial r^2}\{u\},
\end{aligned} \tag{5.18}$$

and

$$\Delta_{zr}\{u\} \approx \frac{\partial^2}{\partial r\,\partial z}\{u\}$$

represent the finite difference approximations. Because the Lagrangian meshes deform, a central finite difference operator is not always suitable. The central difference has been replaced by a contour difference that maintains a second order accuracy.

The finite difference operator is not optimally stable. The maximum value of the

time step is restricted by the following equation.

$$\frac{\Delta t}{\min(\Delta z, \Delta r)} \max(\lambda_A, \lambda_B) < \frac{1}{\sqrt{8}}$$

where λ_A, λ_B are the eigenvalues of A and B respectively. In an optimally stable scheme, the right hand side, which is also often called Courant, Friedrichs and Levy number (CFL), should be 1, instead of $1/\sqrt{8}$. Furthermore the operator (5.17) is complicated and the increased number of computations, in many cases, negates any computational efficiency obtained by resorting to second order accurate methods. The Lax-Wendroff operator can be replaced by a modified Strang's[40,41] operator to make the Lax-Wendroff's scheme optimally stable. The modification of Strang's scheme involves replacing the central difference operators of Strang by contour differences and accomodating the axisymmetric equations. Then,

$$\{u\}^{t+\Delta t} = L_r^{\Delta t/2} L_z^{\Delta t/2} L_z^{\Delta t/2} L_r^{\Delta t/2} \{u\}^t \tag{5.19}$$

where

$$\begin{aligned} L_z^{\Delta t/2} = {} & [I] + \frac{\Delta t}{2}([A]\Delta_z + [D]\Delta_o) \\ & + \frac{\Delta t^2}{4}\Big\{[A]^2\Delta_z\Delta_z + ([A][D] + [D][A] \\ & + [A][A]_{,u}\Delta_z + [A]_{,u}[A]\Delta_z + [A]_{,u}[D]_{\ o})\Delta_z \\ & + ([D]^2 + [A][D]_{,u}\Delta_z + [D]_{,u}[A]\Delta_z + [D]_{,u}[D]\Delta_o)\Big\} \end{aligned} \tag{5.20}$$

$$L_r^{\Delta t/2} = [I] + \frac{\Delta t}{2}([B]\Delta_r + [E])$$

$$+ \frac{\Delta t^2}{4}\Big\{[B]^2\Delta_{rr} + ([B][E] + [E][B] + [B][B]_{,u}\Delta_r$$

$$+ [B]_{,u}[B]\Delta_r + [B]_{,u}[E]\Delta_o)\Delta_r + ([E][E] + [B][E]_{,u}\Delta_r$$

$$+ [E]_{,u}[B]\Delta_r + [E]_{,u}[E]\Delta_o)\Big\} \qquad (5.21)$$

and

$$[D] + [E] = [C] \quad . \qquad (5.22)$$

Even though the Strang's type of operator (5.20) is optimally stable, the computational efficiency can be substantially increased by restoring the second order accuracy at every other time step by following the procedures similar to those of Gourlay, Morris and Mitchell[42,43]. Then

$$L_{rz}^{t+2\Delta t} = L_r^{\Delta t} L_z^{\Delta t} L_z^{\Delta t} L_r^{\Delta t}\{u\} \quad . \qquad (5.23)$$

The finite difference operators (5.23), (5.20) and (5.21) still contain multiplication of matrices, such as, $[A][B]$, $[A]_{,u}[A]$ etc. The operation can be simplified by using two step procedures[44]. Thus, for example

$$L_z^* = [I] + \Delta t[A]\Delta_z + \Delta t[D]$$

$$L_z = \frac{1}{2}([I] + L_z^*) + \frac{\Delta t}{2}([A]^*\Delta_z + [D]^*) \qquad (5.24)$$

where $[A]^*$ and $[D]^*$ are evaluated by using the value of $\{u\}^*$. A similar expression can be written for L_r in r-direction. Suitable spatial contour difference forms that maintain second order accuracy and are suitable for use in equations of the type (5.24) have been developed at Georgia Institute of Technology*. These are different from those used in references (28, 29)

For an interior point, a typical member V of the field vector $\{u\}$ is evaluated as follows.

$$
\begin{aligned}
V_{(1)} &= U^t + \Delta t(B\,\Delta_r + E)\,U^t \\
V_{(2)} &= \tfrac{1}{2}(U^t + V_{(1)}) + \tfrac{1}{2}\Delta t(B_{(1)}\nabla_r + E_{(1)})\,V_{(1)} \\
V_{(3)} &= V_{(2)} + \Delta t(A_{(2)}\Delta_z + D_{(2)})\,V_{(2)} \\
V_{(4)} &= \tfrac{1}{2}(V_{(2)} + V_{(3)}) + \tfrac{\Delta t}{2}(A_{(3)}\nabla_z + D_{(3)})\,V_{(3)} \\
V_{(5)} &= V_{(4)} + \Delta t(A_{(4)}\Delta_z + D_{(4)})\,V_{(4)} \\
V_{(6)} &= \tfrac{1}{2}(V_{(4)} + V_{(5)}) + \tfrac{1}{2}\Delta t(A_{(5)}\nabla_z + D_{(5)})\,V_{(5)} \\
V_{(7)} &= V_{(6)} + \Delta t(B_{(6)}\Delta_r + E_{(6)})\,V_{(6)} \\
V_{(8)} &= \tfrac{1}{2}(V_{(6)} + V_{(7)}) + \tfrac{1}{2}\Delta t(B_{(7)}\nabla_r + E_{(7)})\,V_{(7)} \\
U^{t+2\Delta t} &= V_{(8)}
\end{aligned}
\qquad (5.25)
$$

In this equation Δ_r and ∇_r represent the contour difference operators that represent the equivalent forward and backward difference operators, that are needed in the two step

*Chen, H. P., Ph.D. Thesis

procedures. At the boundaries, these equations have been modified to include the appropriate boundary conditions.

5.4 Numerical Results and Discussion

The material considered for the detailed numerical analysis has the following properties:

Solid density, ρ_ℓ = 2.72 gms/cc
Young's Modulus, E = 1.1×10^7 psi (75845 MPa)
Poisson's ratio, ν = 0.3

In the following analysis, three different types of material behavior have been considered. These are: (i) elastic behavior, (ii) elastic-plastic behavior and (iii) elastic-plastic behavior in a locking material. For the study, a yield stress Y = 20,000 psi (137.9 MPa) has been assumed. For the locking material, the initial density is chosen to be 2.1 gms/cc. There are three distinct branches of the pressure-density relationship. These are shown in Figure 5.1. For this analysis, first two branches are assumed to be straight line segments. The values chosen for ρ_o, ρ_1, p_1 etc. (figure 5.1), for the present numerical studies, are

ρ_o = 2.1 gms/cc $\qquad$ p_1 = 6600 psi (45.5 MPa)

ρ_1 = 2.11 gms/cc $\qquad$ p_ℓ = 66600 psi (459.2 MPa)

and

ρ_ℓ = 2.72 gms/cc .

The equations of the lines corresponding to the three branches of the pressure-density relations are

$$p = \frac{p_1}{\rho_1 - \rho_o} (\rho - \rho_o) \qquad \rho \leq \rho_1$$

$$p = p_1 + \frac{p_o - p_1}{\rho_o - \rho_1} (\rho - \rho_1) \qquad \rho_1 < \rho < \rho_\ell$$

$$p = A(\rho/\rho_G - 1) + B(\rho/\rho_G - 1)^2 \qquad \rho > \rho_\ell \quad .$$

The constants A, B, ρ_G are selected from reference 3.

Two different time variations of loading are considered. The first type is a step loading (without unloading) as shown in Figure 5.2. The second type is also a step loading but with an unloading at a time $t = \bar{t}$. This is shown in Figure 4.1. The magnitude of the peak compressive stress σ_o has been assumed to be 100,000 psi (689.5 MPa). The geometry of the structure and the corresponding applied loading are shown in Figures 5.3a and 5.3b. The boundary conditions at the unloaded edges are also shown in the same figures. These boundary conditions are the same for both the cases of applied loading. Physically, these boundaries can be considered to be "frictionless-rigid". This means that, on these edges, the velocities in the direction normal to the plane of edges and the shear stresses are zero. Referring to figures 5.3a and 5.3b, these boundary conditions are expressed as $w = 0$, $\tau_{zr} = 0$ at the boundary which can be denoted by $z(t = 0) = L$ and $u = 0$, $\tau_{zr} = 0$ at the boundary denoted by $r(t = 0) = R$. On the left boundary, represented by $z(t = 0) = 0$, there are two types of applied loading. One type corresponds to the load on the entire edge as shown in Figure 5.3a and the other corresponds to a partial load on the edge as shown in Figure 5.3b. There are two cases of loading type shown in Figure 5.3a. These cases are denoted as case 5a and case 5b. In both these cases, the loading, the geometry and the boundary conditions are such that a one-dimensional strain condition is created in the axisymmetric problem that consists of two space dimensions and time. The problems under these cases are solved in order to simulate a one-dimensional problem of transient dynamic analysis that can be compared with known solutions. The difference between case 5a and case 5b is that case 5a has only a step loading while case 5b has a step loading followed by a step unloading. The case 5b can also be called a pulse loading.

Similar to the above cases, there are also two different cases under the partial loading condition shown in Figure 5.3b. These cases are identified as case 5c and case 5d. The partial loading creates two-dimensional conditions. Again, the difference between case 5c and case 5d is that case 5c represents a step loading and case 5d represents a pulse loading.

The dimensions pertaining to the problem are as follows (Figure 5.3)

$$L = 3.2 \text{ in (81 mm)}, \; R = 0.8 \text{ in (20 mm)}, \; R_1 = 0.32 \text{ in (8 mm)}$$

In order to apply the finite difference scheme, the region bounded internally by the edges $z(t = 0) = 0$, L and $r(t = 0) = 0$, R is divided into 400 cells. The dimensions of these cells are: $\Delta z = \Delta r = 0.08$ in (2 mm). This mesh pattern is used for all the cases. Since the finite difference scheme proposed in this section is optimally stable, the CFL number is chosen to be 1. However, the time step Δt is not always a constant. All the plots display the variation of the stress σ_{zz} with repsect to the deformed z-coordinate. Also, the symbols E, E-P and E-P-L in the figures refer to the elastic solid, elastic-plastic solid and elastic-plastic-locking material respectively.

As a first step, some typical results of the stress variations obtained by using a leap frog scheme (programed at Georgia Institute of Technology) with linear or quadratic artificial viscosities are compared with those obtained by the second order accurate method. These are shown in Figures 5.4a, 5.4b and 5.4c. In these figures, step loading condition of case 5a has been assumed and only elastic behavior is considered. The addition of artificial viscosity in a leap frog scheme results in a scheme that is no longer optimally stable. Suitable CFL numbers must be chosen in these numerical calculations. In Figure 5.4a the descriptions of the plots correspond to the CFL numbers and times t as given in the following table.

Method used	CFL number	Elapsed time t after the application of load
present method	1.0	9.25 μsecs
leap frog scheme with linear viscosity	0.3334	9.26 μsecs
leap frog scheme with quadratic viscosity	0.3334	9.51 μsecs

It can be seen from Figure 5.4a that the σ_{zz} - z variation by the present second order accurate method has a very sharp wave front, and indicates very little oscillation behind the shock wave. A modest amount of overshooting of the shock front can also be observed. The curve obtained by leap frog scheme with linear viscosity has a very wide

transition layer instead of a steep shock front, although it has no overshooting and oscillations behind the shock wave. In the plot that represents the results of the leap frog scheme with quadratic viscosity, oscillations behind the shock wave are significant. The solution represents a problem with one-dimensional strain and hence no physically significant oscillations are present. All oscillations are computationally induced. A larger overshooting is observed when compared with that of the second order accurate method. The shock wave front is also not steep. The results of using higher CFL numbers in the leap frog scheme with artificial viscosity are shown in Figures 5.4b and 5.4c. For the results shown in Figure 5.4b, the CFL number used is 0.66 for both the linear and quadratic viscosity cases. Obviously, the results indicate instability. Oscillations behind the wave front, large overshooting and wide transition shock layers can be observed. In Figure 5.4c, the values of CFL = 0.7 and 0.9 are used in the leap frog scheme with linear and quadratic viscosities respectively. These results are also not satisfactory because of the numerical instability. From this elementary analysis, it can be concluded that the second order accurate finite difference method suggested in this report is a desirable choice for using larger time steps.

Elastic, elastic-plastic and elastic-plastic locking behavior are compared in Figures 5.5 and 5.6. In both these figures, the stress σ_{zz} has been plotted against the current z coordiantes that were originally located along $r(t = 0) = 0$. The Figure 5.5 corresponds to approximately 7 μsecs after loading at the boundary $z(t = 0) = 0$. The corresponding time for Figure 5.6 is approxiamtely equal to 12 μsecs. The specific times for the elastic body, elastic-plastic and elastic-plastic-locking bodies in the Figure 5.5 are 6.61 μsecs, 6.60 μsecs and 6.74 μsecs. Similar times in Figure 5.6 are 11.09 μsecs for the elastic body, 11.86 μsecs for the elastic-plastic body and 11.96 μsecs for the elastic-plastic locking material. The calculated values were available at these different times because of the different values of Δt. The three different wave fronts can be seen for the elastic-plastic locking material. The single wave front for the elastic body and a two wave front system for elastic-plastic body can also be seen. There are no oscillations behind the wave front because of the simulation of one-dimensional strain conditions by a combination of loading, geometry and boundary conditions. The velocity of the locking wave is the slowest of the waves.

In Figure 5.7, the results for the case of a pulse loading are shown. The loading consists of a step loading followed by a step unloading. Again the loading, geometry and the boundary conditions simulate the one-dimensional strain conditions. The applied load

is set to zero at $t = \bar{t}$. The value of $\bar{t} = 1.33$ μ secs for the elastic body, $\bar{t} = 1.33$ μ secs for the elastic-plastic body and $\bar{t} = 1.42$ μ secs for the elastic-plastic locking material have been selected. The figure clearly indicates that the attenuation of peak stresses is maximum in the locking material. A reduction of peak stress is also seen in the elastic-plastic body without locking. The reduction, however, is not significant in comparison to the locking material. In the elastic body the peak stresses are not reduced. These results support the fact that locking materials are effective stress attenuators.

The loading for cases 5c and 5d correspond to a partial loading on the surface $z(t = 0) = 0$. This corresponds to a two-dimensional (r - z) problem. The variation of σ_{zz} against z are shown in Figures 5.8 to 5.10. These are for a step loading without unloading. The two Figures 5.8 and 5.9 correspond to lines $r(t = 0) = 0$ and 0.56 in (14.2 mm). It is observed that the elastic-plastic locking material displays a steeper wave front in comparison with an elastic-plastic material. The oscillations behind the elastic wave, due to boundary effects in this two-dimensional problem, can be seen. The stress magnitudes in Figure 5.9 are small. This is due to the fact that the region is away from the area of the load application. The variations of σ_{zz} with z, for $r(t = 0) = 0$ and the locking material, are shown in Figure 5.10 for increasing values of times. The development of three distinct wave fronts can be seen.

The Figures 5.11 and 5.12 correspond to pulse loadings on a part of the surface specified by $z(t = 0) = 0$. Again, two-dimensional effects are present. The Figure 5.11 is for $r(t = 0) = 0$. The Figure 5.12 is for $r(t = 0) = 0.56$ in (14.2 mm) which is located away from the loading region. Again, observation regarding the attenuation of peak stresses can be made.

6. CONCLUSIONS

In this report, it has been shown that a locking material shield has the potential of protecting a given structure from dynamic loads that have a time history similar to that of mine blasts. This conclusion is based on the analysis under conditions of one-dimensional strain and the studies under conditions of axisymmetry. In order to provide a tool for designing the locking material shield, a second order accurate, computationally efficient numerical scheme has been developed. The numerical scheme is capable of considering large deformations and locking phase transition and provide accurate results in comparison to the present state-of-the-art. Point condition codes are also developed for locking material-structure combinations. The accuracy and the reliability of the resulting computer program have been checked by comparing the results with known

solutions.

To follow the present work, some additional tasks are recommended. One such task is to improve the accuracy and the computational efficiency during phase transition and unloading. Furthermore, the shockwave can be steepened by employing new techniques such as the method of artificial compression. Another area of suggested work is the non-ideal plasticity. A very important additional task will be to investigate the accuracy of methods such as the state space approach with its inherent exactness and simplicity of reducing three-dimensional problems to those involving only two-dimensions.

REFERENCES

1. Hanagud, S., "A Contribution to the Theory of Isotropic Licking" Sudaer Report No.152, Stanford University, California, 1963.

2. Hanagud, S., "Finite Amplitude Spherical Shock Waves in Locking Solids" Proc. 5th U.S. National Congress, 1966. (Invited Sectional Lecture).

3. Linde, R. K., and D. N. Schmidt, "Attenuation of Shockwaves in Distended Solids" AFWL-TR-66-13, 1966.

4. Hanagud, S., G. S. Sidhu and B. Ross, "Elastic-Plastic Impact of Compactible Rods and Plates" Israel Journal of Technology, 1969.

5. Miklowitz, J., The Theory of Elastic Waves and Waveguides, North-Holland, 1978.

6. Achenbach, J. D., "Wave Propagation, Elastodynamic Stress Singularities, and Fracture", Theoretical and Applied Mechanics, ed. W. T. Koiter, North-Holland Publishing, 1976, pp. 71-87.

7. Fung, Y. C., Foundations of Solid Mechanics, Prentice-Hall, 1965.

8. de Hoop, A. T., "A Modification of Cagniard's Method for Solving Seismic Pulse Problems", Appl. Sci. Res., Sec. B, 8, 1959, pp. 349-356.

9. Ang, D. D., "Transient Motion of a Line Load on the Surface of an Elastic Half-Space", Quart. Appl. Math., 18, 1960, pp. 251-256.

10. Mitra, M., "Disturbance Produced in an Elastic Half-Space by Impulsive Normal Pressure", Proc. Camb. Phil. Soc., 60, 1964, pp. 683-696.

11. Norwood, F. R., "Exact Transient Response of an Elastic Half Space Loaded Over a Rectangular Region of its Surface', J. Appl. Mech., 36, 1969, pp. 516-522.

12. Gakenheimer, D. C., and J. Miklowitz, "Transient Excitation of an Elastic Half Space by a Point Load Traveling on the Surface", J. Appl. Mech., 36, 1969, pp. 505-515.

13. Gakenheimer, D. C., "Numerical Results for Lamb's Point Load Problem", J. Appl. Mech., 37, 1970, pp. 522-524.

14. Chao, C. C., "Dynamical Response of an Elastic Half-Space to Tangential Surface Loadings", J. App. Mech., 27, 1960, pp. 559-567.

15. Eason, G., "The Displacements Produced in an Elastic Half-Space by a Suddenly Applied Surface Force", J. Inst. Maths. Applics., 2, 1966, pp. 299-326.

16. Craggs, J. W., "On Axially Symmetric Waves", Proc. Camb. Phil. Soc., 59, 1963, pp. 803-809.

17. Craggs, J. W., "On Two-Dimensional Waves in an Elastic Half-Space", Proc. Cambridge Phil. Soc., 56, 1960, pp. 269-285.

18. Eason, G., "The Stress Produced in a Semi-Infinite Solid by a Moving Surface Force", Int. J. Engng. Sci., 2, 1965, pp. 581-609.

19. Ungar, A., "The Propagation of Elastic Waves from Moving Normal Point Loads in Layered Media", Pageoph, 114, 1976, pp. 845-861.

20. Miles, J. W., "Homogeneous Solutions in Elastic Wave Propagation", Quart. Appl. Math., 18, 1960, pp. 37-59.

21. Norwood, F. R., "Interior Motion of an Elastic Half-Space Due to Normal Finite Moving Line Load on its Surface", Int. J. Solids Struct., 6, 1970, pp. 1483-1498.

22. Handelman, G. H., and L. A. Rubenfeld, "Diffraction of Horizontal Shear Waves by a Half Plane", J. Appl. Mech., 36, 1969, pp. 873-874.

23. Butler, D. S., "The Numerical Solution of Hyperbolic System of Partial Differential Equations in Three Independent Variables" Proc. Royal, Soc. (London), Series A, 17, 1964, pp. 381-398.

24. Clifton, R. J., "A Difference Method for Plane Problems in Dynamic Elasticity", Quart. Appl. Math., 25, 1968, pp. 97-116.

25. Hanagud, S., and R. L. Latham, "Interaction of Stress Waves and Cracks", Technical report, Georgia Institute of Technology (AFOSR Grant, 1982)

26. Von Neumann, J. and R. Richtmyer, "A Method for the Numerical Calculation of Hydrodynamic Shocks", J. Appl. Phys., 21, 1950, pp. 232-237.

27. Roache, P. J., Computational Fluid Dynamics, 2nd edition, Hermosa, 1976.

28. Wilkins, M., "Finite Difference Scheme for Calculating Problems in Two Space Dimensions and Time", J. Comput. Phys., 5, 1970, pp. 406-414.

29. Chen, Y. M., and M. L. Wilkins, "Numerical Analysis of Dynamic Crack Problems", Elastodynamic Crack Problems, ed., G. C. Sih, Noordhoff, 1977, p. 295-345.

30. Richtmyer, R. D., and K. W. Morton, Difference Methods for Initial Value Problems, 2nd edition, Interscience-Wiley, 1967.

31. Wilkins, M. L., "Calcualtion of Elastic-Plastic Flow", Methods in Computational Physics, 3, 1964, Academic Press, pp. 211-263.

32. Andrews, D., "A Numerical Study of Tectonic Stress Release by Underground Explosions", Bull. Seismol. Soc. Am., 63, No. 4, pp. 1375-1391.

33. Andrews, D., "Rupture Propagation With Finite Stress in Antiplane Strain", Journal of Geophysical Research, 81, No. 20, 1976, pp. 3575-3582.

34. Madariaga, R., "Dynamics of an Expanding Circular Fault", Bull. Seism. Soc. Am., 66, No. 3, 1976, pp. 639-666.

35. Alterman, Z. and F. Karal, "Propagation of Elastic Waves in Layered Media by Finite Difference Methods", Bull. Seismol. Soc. Am., 58, No. 1, pp. 367-398.

36. Hanagud, S., B. Ross and G. S. Sidhu, "Axisymmetric Impact of Compactible Rods Subjected to Large Deformations", Israel J. of Technology, 1972.

37. Lax, P., and B. Wendroff, "Difference Schemes for Hyperbolic Equations with High Order of Accuracy", Comm. Pure Appl. Math., 17, 1964, pp. 381-398.

38. Gottlieb, D., "Strang-Type Difference Schemes for Multidimensional Problems", SIAM J. Numer. Anal., 9, 1972, pp. 650-661.

39. Smith, P. D., "On Some Numerical Schemes for the Solution of Wave Propagation Problems", Int. J. Num. Meth. Engng., 8, 1974, pp. 91-102.

40. Strang, G., "On the Construction and Comparison of Difference Schemes", SIAM J. Numer. Anal. 5, No. 3, 1965, pp. 506-517.

41. Strang, G., "Accurate Partial Difference Methods I: Linear Cauchy Problems", Arch. Rat. Mech. Anal., 12, 1963, pp. 392-402.

42. Gourlay, A. R., and J. L. Morris, "On the Comparison of Multistep Formulations of the Optimized Lax-Wendroff Method for Nonlinear Hyperbolic Equations in two Space Dimensions", J. Comp. Phys., 5, 1970, pp. 229-243.

43. Gourlay, A. R., and A. R. Mitchell, "A Classification of Split Difference Methods for Hyperbolic Equations in Several Space Dimensions". SIAM J. Numer. Anal., 6, No. 1, 1966, pp. 62-71.

44. MacCormack, R. W., and A. J. Paullay, "The Influence of the Computational Mesh on Accuracy for Initial Value Problems with Discontinuous or Nonunique Solutions", Comp. Fluids, 2, 1974, pp. 339-361.

45. Gottlieb, D., and Turkel, E., "On Acceleration of MacCormack's Scheme", J. Comp. Phys., 26, 1978, pp. 252-256.

46. Glimm, J., "Solution in the Large for Nonlinear Hyperbolic Systems of Equations", Comm. Pure Appl. Math., 18, 1965, pp. 697-715.

47. Chorin, J. A., "Random Choice Solution of Hyperbolic Systems", J. Comp. Phys., 22, 1976, pp. 517-533.

48. Harten, A., "The Artifical Compression Method for Shocks and Contact Discontinuities", Comm. Pure Appl. Math., 30, 1977, pp. 611-630.

49. Harten, A., "The Method of Artificial Compression" U.S. Atomic Energy Commission, contract report-(11-1)-3077, 1979.

50. Gottlieb, D. and Turkel, E., "Boundary Conditions for Multistep Finite-Difference Methods for Time-Dependent Equation", J. Comp. Phys., 26, 1978, pp. 181-196.

51. McGuire, G. R., and Morris, J. L., "Restarting Order of Accuracy for Multilevel Scheme for Nonlinear Hyperbolic System in Many Variables", J. Inst. Math. Appl., 17, 1976, pp. 53-67.

52. Varley, E. (Ed.), "Propagation of Shcok Waves in Solids", AMD, 17, ASME, New York 1976.

53. Truesdell, C. (Ed.) Continuum Mechanics III, Foundations of Elasticity Theory, International Science Review Series, 1965.

Fig.1.1 A Simple Locking Material

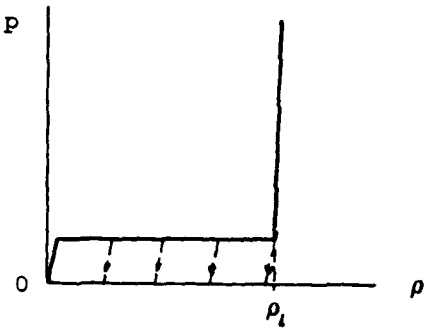

Fig.1.2 An Elastic Locking Solid

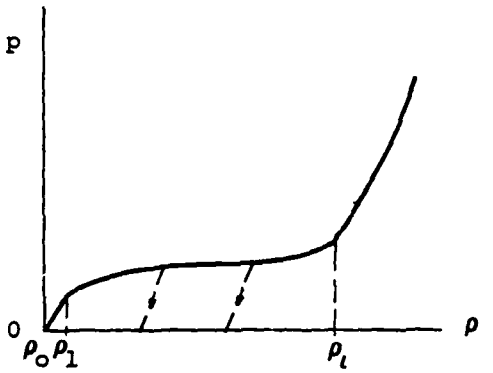

Fig.1.3 Experimental p-ρ diagram for Locking Materials

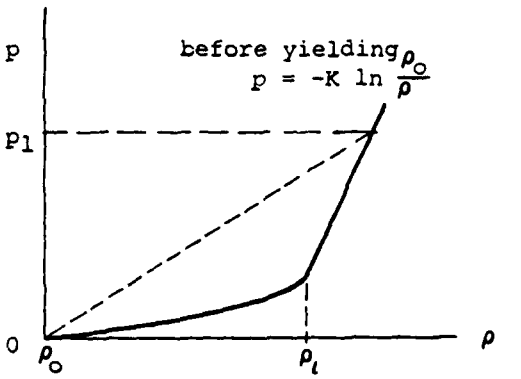

Fig.1.4 Pressure-Density Relationship

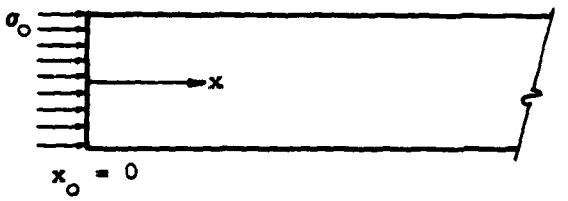

Fig.1.5 Material Geometry and Loading

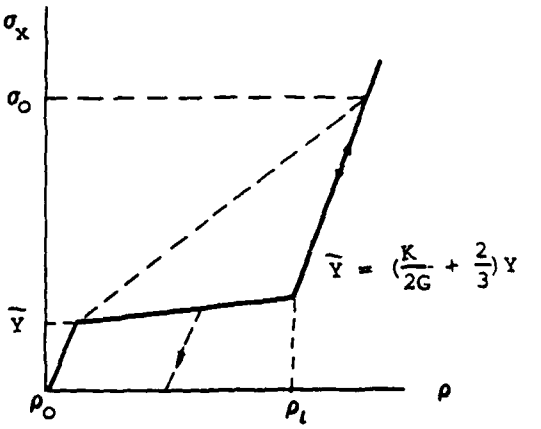

Fig.1.6 σ_x - ρ Relationship

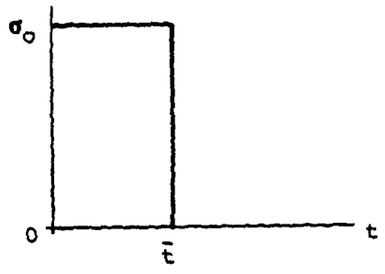

Fig.4.1 Step Loading - Case 'a'

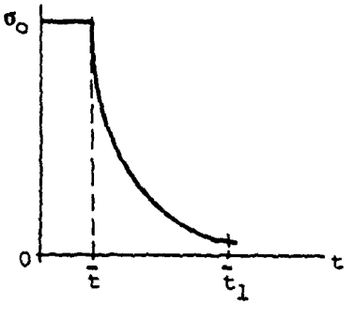

Fig.4.2 Step Loading - Case 'b'

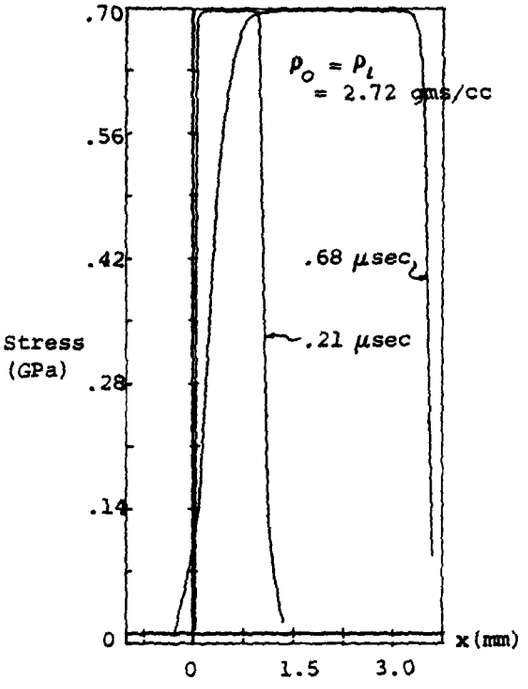

Fig.4.3 Stress Distribution
(Loading 'a')

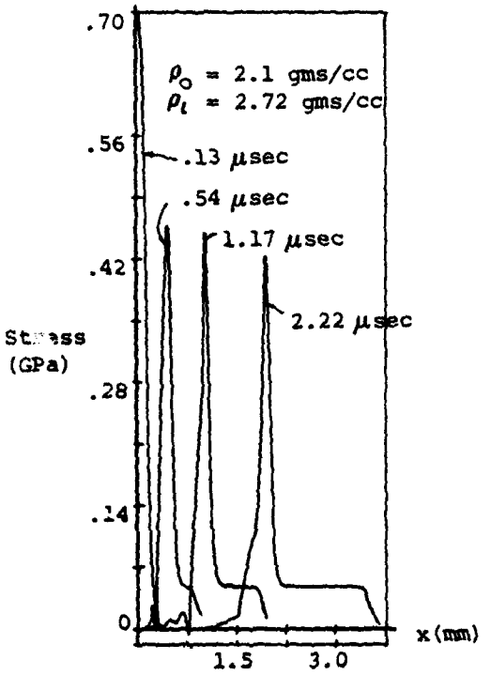

Fig.4.4 Stress Distribution
(Loading 'a')

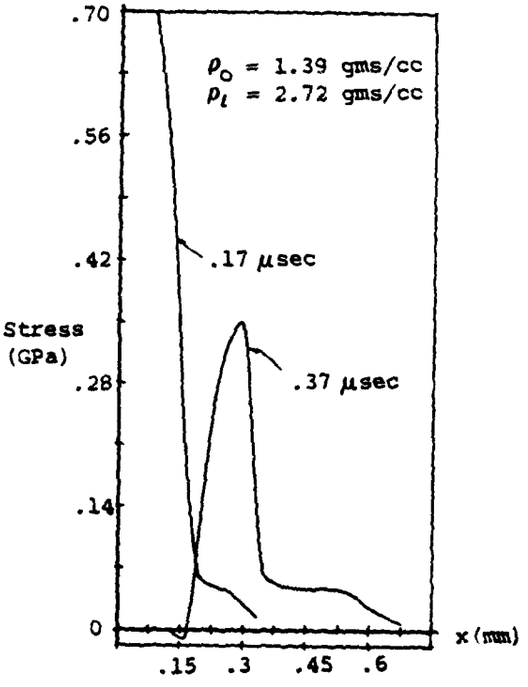

Fig.4.5 Stress Distribution
(Loading 'a')

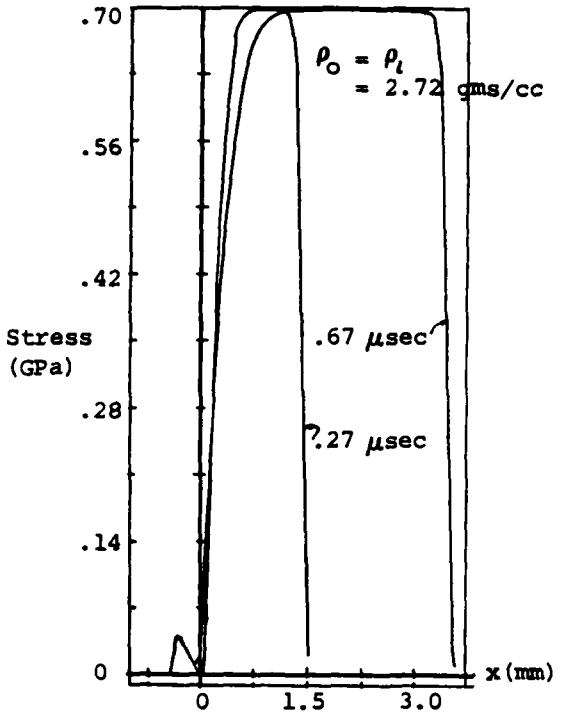

Fig.4.6 Stress Distribution
(Loading 'b')

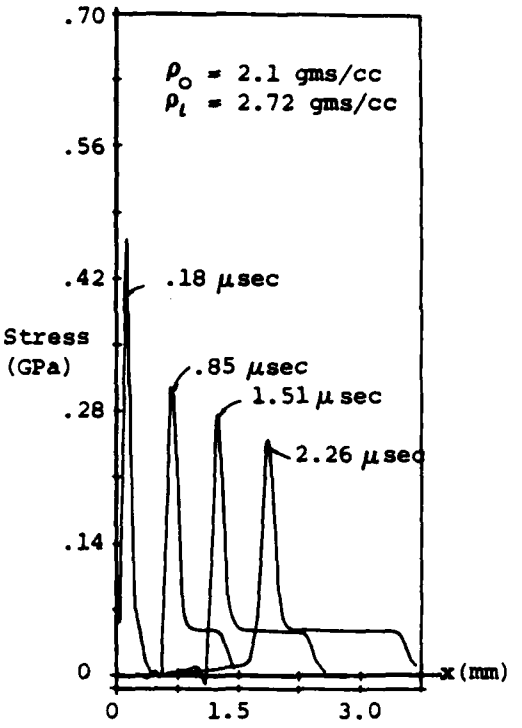

Fig.4.7 Stress Distribution
(Loading 'b')

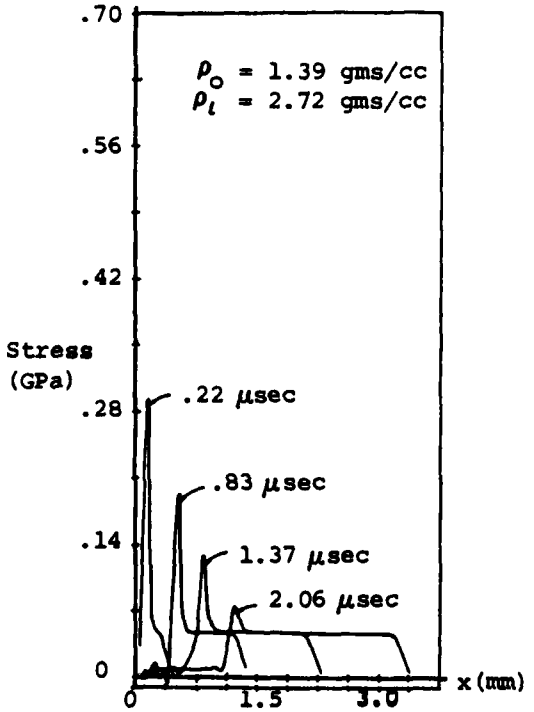

Fig.4.8 Stress Distribution
(Loading 'b')

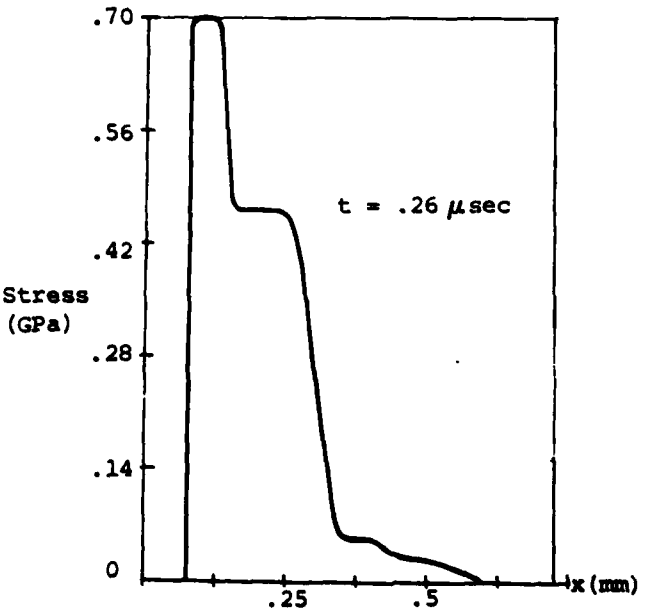

Fig.4.9 Plasticity Effects
(Yield Stress = .56 GPa)

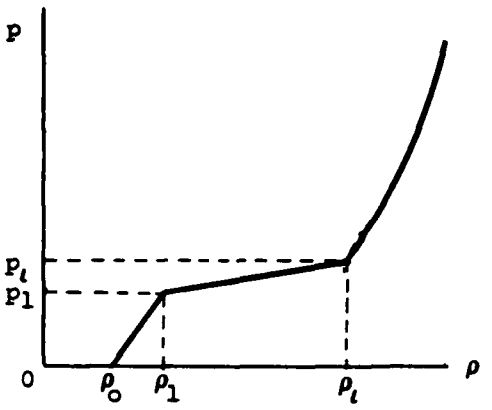

Fig.5.1 Simplified p - ρ Relationship

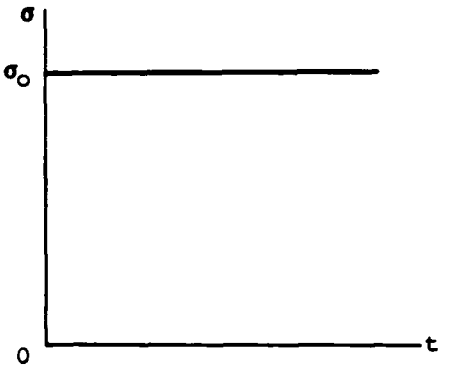

Fig.5.2 Step Loading without Unloading

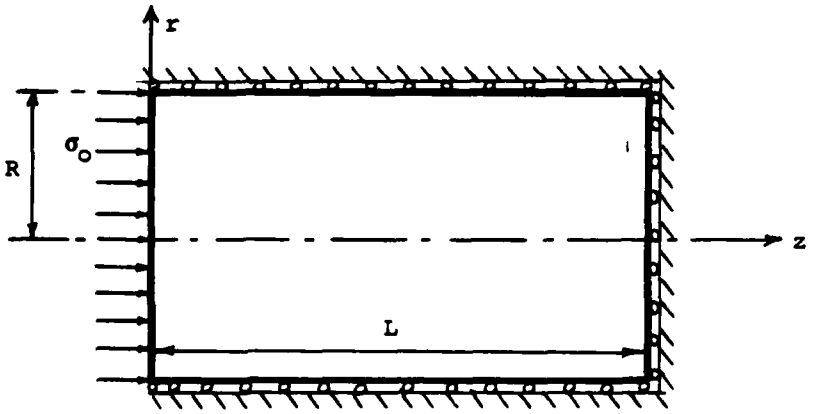

Fig.5.3a Geometry and Loading with Fully Loaded Edge

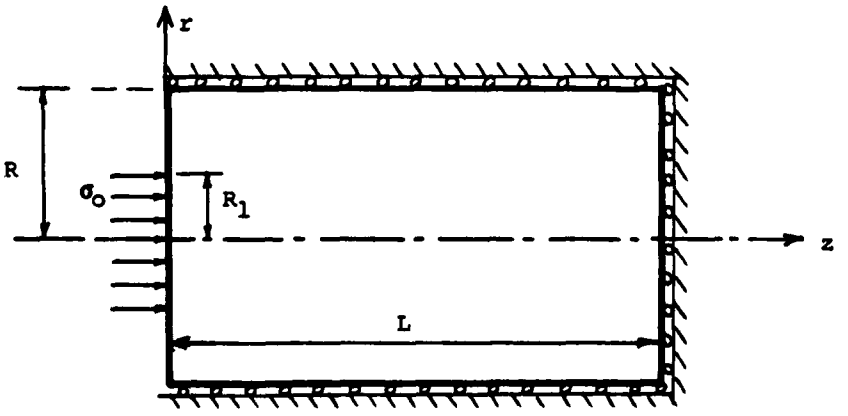

Fig.5.3b Geometry and Loading with Partially Loaded Edge

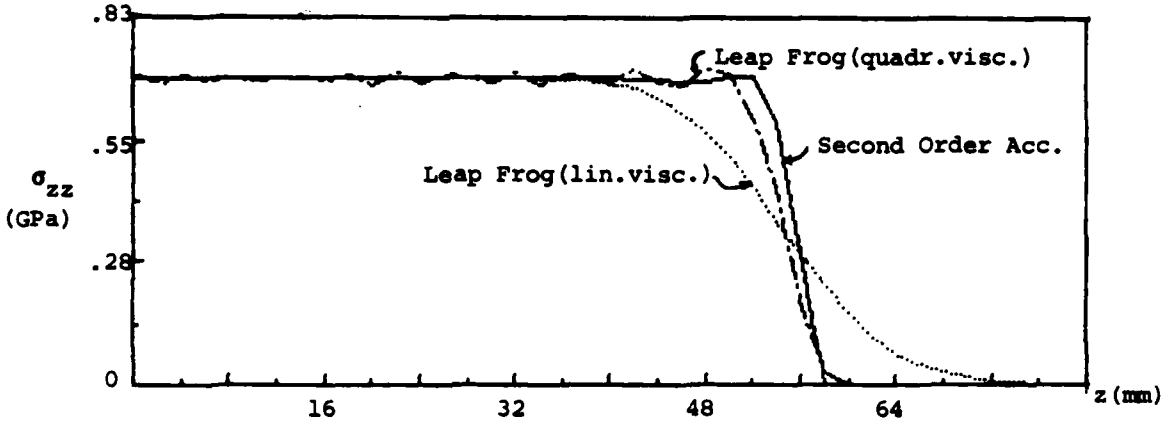

Fig.5.4a σ_{zz} - z Variation with Different Schemes (Elastic Case)

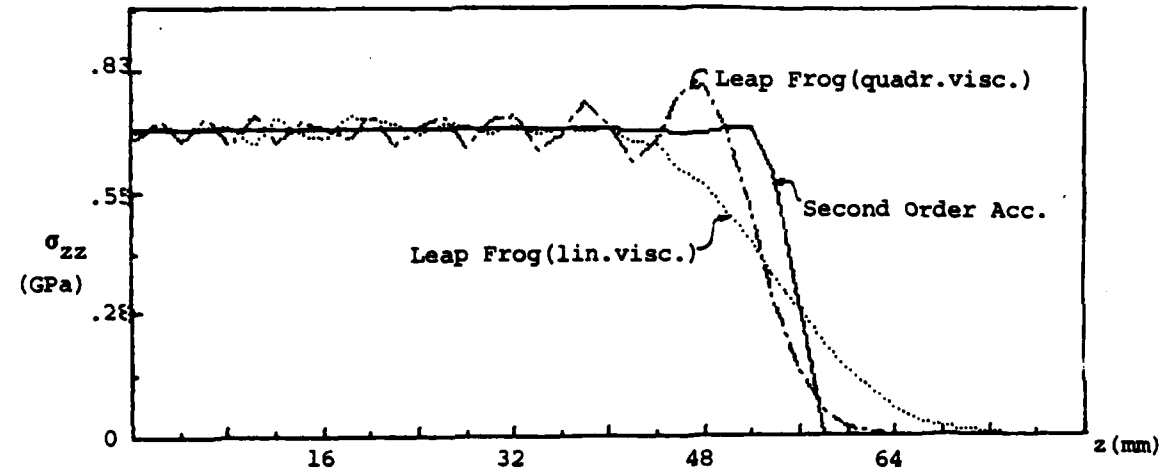

Fig.5.4b σ_{zz} - z Variation with Different Schemes (Elastic Case)

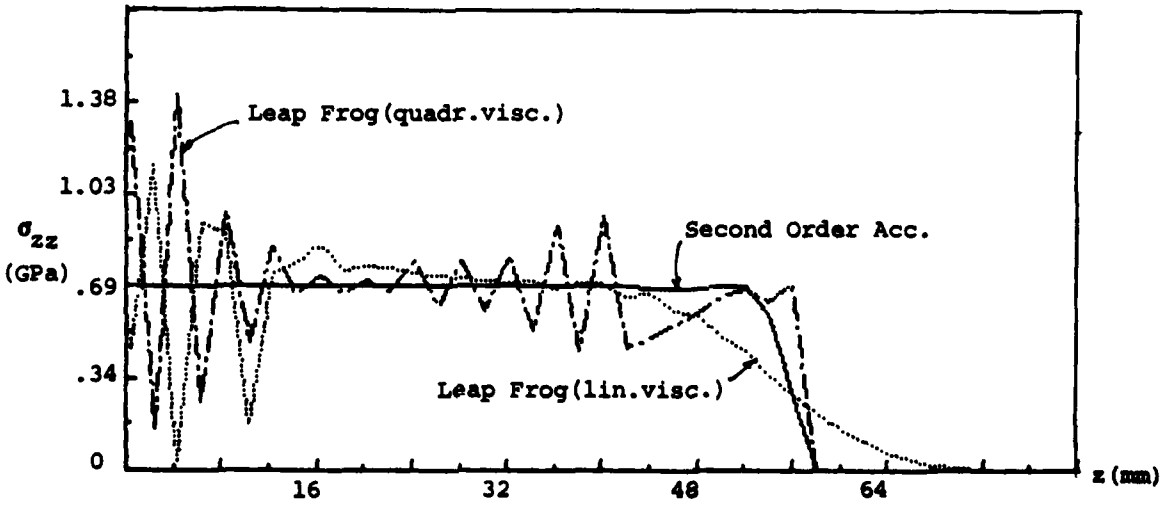

Fig.5.4c σ_{zz} - z Variation with Different Schemes (Elastic Case)

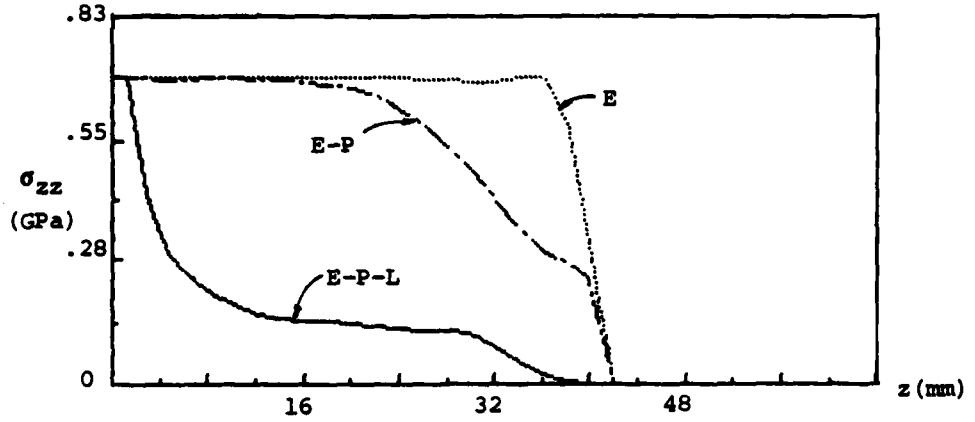

Fig.5.5 σ_{zz} - z Variation for Step Loading

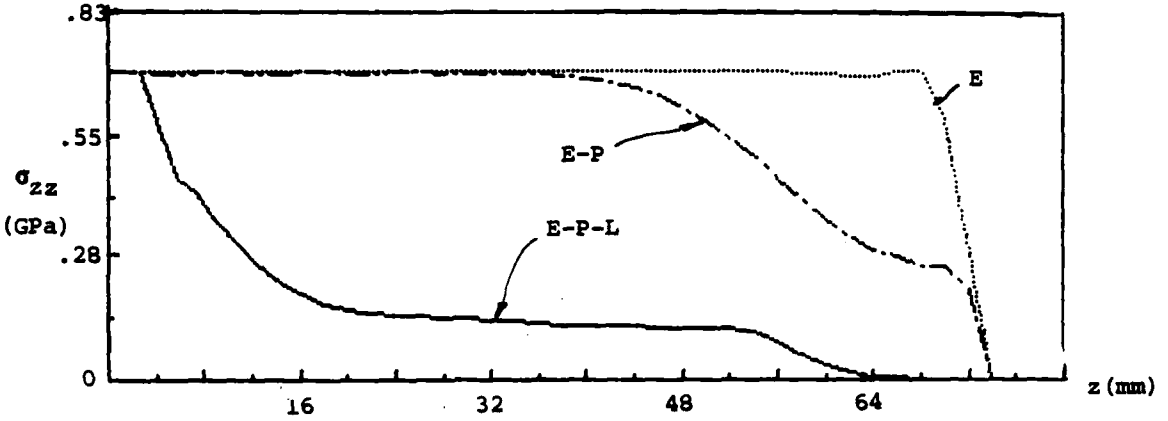

Fig.5.6 σ_{zz} - z Variation for Step Loading

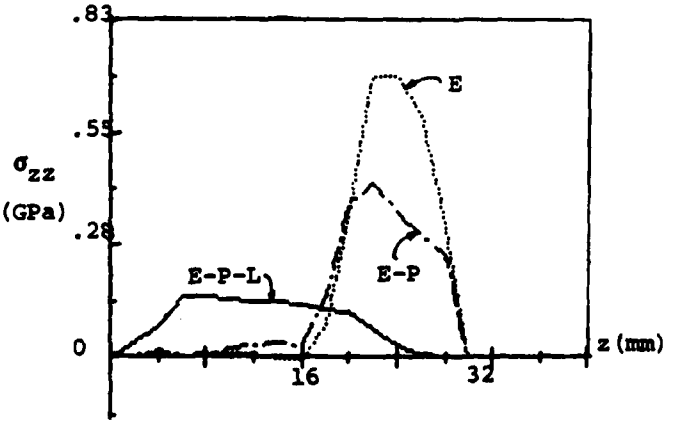

Fig.5.7 σ_{zz} - z Variation for Pulse Loading

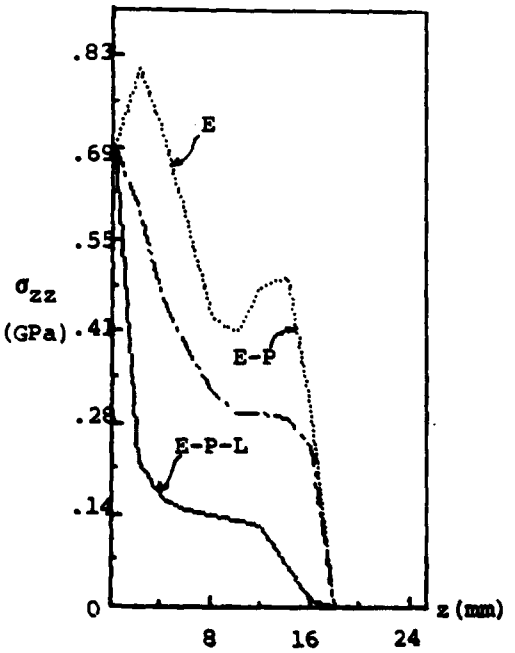

Fig.5.8 σ_{zz} - z Variation for Step Loading

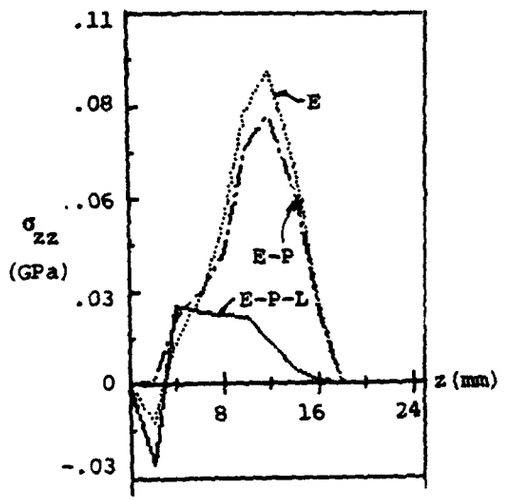

Fig.5.9 σ_{zz} - z Variation for Step Loading

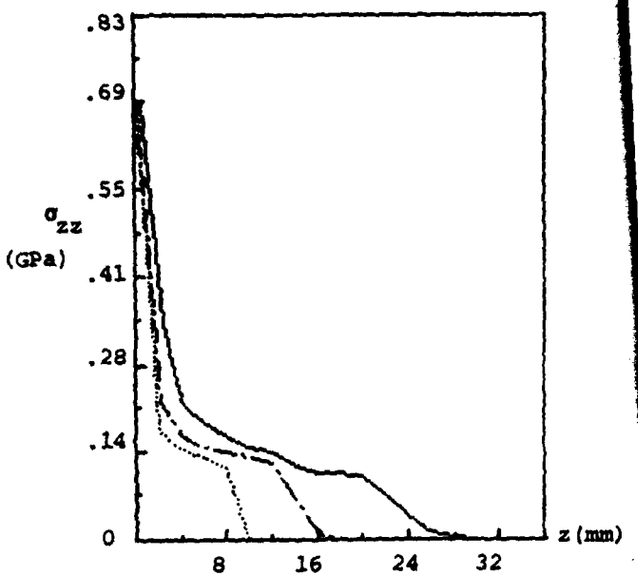

Fig.5.10 σ_{zz} - z Variation for Step Loading

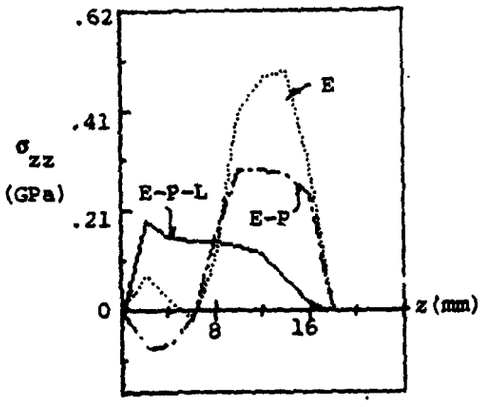

Fig.5.11 σ_{zz} - z Variation for Pulse Loading

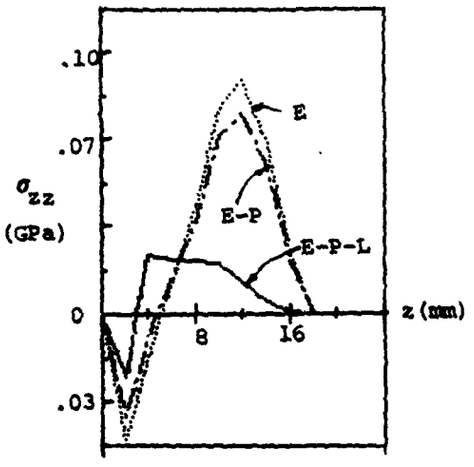

Fig.5.12 σ_{zz} - z Variation for Pulse Loading

DISTRIBUTION LIST

No. of Copies	To
1	Office of the Under Secretary of Defense for Research and Engineering, The Pentagon, Washington, DC 20301
12	Commander, Defense Technical Information Center, Cameron Station, Building 5, 5010 Duke Street, Alexandria, VA 22314
1	Metals and Ceramics Information Center, Battelle Columbus Laboratories, 505 King Avenue, Columbus, OH 43201
1	Deputy Chief of Staff, Research, Development, and Acquisition, Headquarters Department of the Army, Washington, DC 20301
1	ATTN: DAMA-ARZ
	Commander, Army Research Office, P.O. Box 12211, Research Triangle Park, NC 27709
1	ATTN: Information Processing Office
1	Dr. F. W. Schmiedeshoff
	Commander, U.S. Army Materiel Development and Readiness Command, 5001 Eisenhower Avenue, Alexandria, VA 22333
1	ATTN: DRCLDC
	Commander, U.S. Army Materiel Systems Analysis Activity, Aberdeen Proving Ground, MD 21005
1	ATTN: DRXSY-MP, H. Cohen
	Commander, U.S. Army Communications-Electronics Command, Fort Monmouth, NJ 07703
1	ATTN: DRSEL-LE-R
	Commander, U.S. Army Missile Command, Redstone, AL 35809
1	ATTN: DRSMI-TB, Redstone Scientific Information Center
	Commander, U.S. Army Natick Research and Development Laboratories, Natick, MA 01760
1	ATTN: Technical Library
	Commander, U.S. Army Satellite Communications Agency, Fort Monmouth, NJ 07703
1	ATTN: Technical Document Center
	Commander, U.S. Army Tank-Automotive Command, Warren, MI 48090
1	ATTN: DRSTA-RKA
1	DRSTA-UL, Technical Library

No. of Copies	To
	Commander, U.S. Army Armament Research and Development Command, Dover, NJ 07801
2	ATTN: DRDAR-TSS, Technical Library
	Commander, White Sands Missile Range, NM 88002
1	ATTN: STEWS-WS-VT
	Commander, U.S. Army Armament Research and Development Command, Aberdeen Proving Ground, MD 21010
1	ATTN: DRDAR-QAC-E
	Director, U.S. Army Ballistic Research Laboratory, Aberdeen Proving Ground, MD 21005
1	ATTN: DRDAR-TSB-S (STINFO)
	Commander, Harry Diamond Laboratories, 2800 Powder Mill Road, Adelphi, MD 20783
1	ATTN: Technical Information Office
	Commander, Watervliet Arsenal, Watervliet, NY 12189
1	ATTN: DRDAR-LCB, Dr. T. Davidson
	Commander, U.S. Army Foreign Science and Technology Center, 220 7th Street, N.E. Charlottesville, VA 22901
1	ATTN: Mr. Marley, Military Tech
	Director, Eustis Directorate, U.S. Army Air Mobility Research and Development Laboratory, Fort Eustis, VA 23604
1	ATTN: Mr. J. Robinson, DAVDL-E-MOS (AVRADCOM)
	Commander, U.S. Army Engineer Waterways Experiment Station, Vicksburg, MS 39180
1	ATTN: Research Center Library
	Commander, U.S. Army Research and Technology Laboratory, Air Mobility Research and Development Laboratory, Ames Research Center, Moffett Field, CA 94035
1	ATTN: Dr. R. Foye
	Director, Structural Mechanics Research, Office of Naval Research, 800 North Quincy Street, Arlington, VA 22203
1	ATTN: Dr. N. Perrone
	David W. Taylor Naval Ship Research and Development Center, Annapolis, MD 21402
1	ATTN: Dr. H. P. Chu
	Naval Research Laboratory, Washington, DC 20375
1	ATTN: C. D. Beachem, Head, Adv. Mat'ls Tech Br. (Code 6310)
1	Dr. Jim C. I. Chang

No. of Copies	To
	Chief of Naval Research, Arlington, VA 22217
1	ATTN: Code 471
1	Ship Research Committee, Maritime Transportation Research Board, National Research Council, 2101 Constitution Avenue, N.W., Washington, DC 20418
	Commander, U.S. Air Force Wright Aeronautical Laboratories, Wright-Patterson Air Force Base, OH 45433
2	ATTN: AFWAL/MLSE, E. Morrissey
1	AFFDL/FB, Dr. J. C. Halpin
	Air Force Flight Dynamics Laboratory, Wright-Patterson Air Force Base, OH 45433
1	ATTN: AFFDL (FBS), C. Wallace
1	AFFDL (FBE), G. D. Sendeckyj
	National Aeronautics and Space Administration, Washington, DC 20546
1	ATTN: Mr. B. G. Achhammer
	National Aeronautics and Space Administration, Marshall Space Flight Center, Huntsville, AL 35812
1	ATTN: R. J. Schwinghammer, EH01, Dir., M&P Lab
	National Aeronautics and Space Administration, Langley Research Center, Hampton, VA 23665
1	ATTN: Mr. H. F. Hardrath, Mail Stop 188M
1	Dr. R. J. Hayduck, Mail Stop 243
	National Aeronautics and Space Administration, Lewis Research Center, 21000 Brookpark Road, Cleveland, OH 44135
1	ATTN: Dr. J. E. Srawley, Mail Stop 105-1
	Lockheed-Georgia Company, 86 South Cobb Drive, Marietta, GA 30063
1	ATTN: Materials and Processes, Eng. Dept. 71-11, Zone 54
	National Bureau of Standards, U.S. Department of Commerce, Washington, DC 20234
1	ATTN: Mr. J. A. Bennett
	Director, Army Materials and Mechanics Research Center, Watertown, MA 02172
2	ATTN: DRXMR-PL
1	DRXMR-PR
1	DRXMR-K
1	DRXMR-FD
40	DRXMR-SE, Dr. Tsui


DATE
ILME